

AperTO - Archivio Istituzionale Open Access dell'Università di Torino

Describing the vertical root distribution of alpine plants with simple climate, soil, and plant attributes

This is a pre print version of the following article:

Original Citation:

Availability:

This version is available <http://hdl.handle.net/2318/1826841> since 2021-12-20T13:01:40Z

Published version:

DOI:10.1016/j.catena.2021.105305

Terms of use:

Open Access

Anyone can freely access the full text of works made available as "Open Access". Works made available under a Creative Commons license can be used according to the terms and conditions of said license. Use of all other works requires consent of the right holder (author or publisher) if not exempted from copyright protection by the applicable law.

(Article begins on next page)

1 **Describing the vertical root distribution of alpine plants with simple climate, soil, and**
2 **plant attributes**

3

4 Alejandro Gonzalez-Ollauri^{1*}, Csilla Hudek², Slobodan B. Mickovski¹, Davide Viglietti⁴,
5 Nicole Ceretto⁴, Michele Freppaz^{3,4}

6 ¹The BEAM Research Centre, School of Computing, Engineering and Built Environment,
7 Glasgow Caledonian University, Glasgow G40BA, Scotland, UK

8 ²Cranfield Soil and Agrifood Institute, Cranfield University, College Road MK43 0AL
9 Bedford UK

10 ³Research Centre on Natural Risk in Mountain and Hilly Environments, NatRisk, University
11 of Torino, Largo Paolo Braccini 2, 10095 Grugliasco (TO), Italy

12 ⁴Department of Agricultural, Forest and Food sciences, DISAFA, University of Torino, Largo
13 Paolo Braccini 2, 10095, Grugliasco (TO), Italy

14 *Corresponding author: alejandrolauri@gcu.ac.uk

15 **Abstract**

16 The vertical root distribution (VRD) in the soil remains unknown for most plant species, as
17 studying root systems in different pedo-climatic settings is time-consuming and
18 methodologically challenging. Yet, information on the VRD of different vegetation types is
19 essential to understand better the biogeochemical processes occurring at the soil-plant-
20 atmosphere continuum. The aim of this study was to describe the (VRD) of three dominant
21 alpine, herbaceous plants (i.e. *Euphrasia minima* Jacq., *Leucanthemopsis alpina* L., and *Poa*
22 *alpina* L.) on the basis of simple and easy-to-measure climate, soil, and plant attributes in order
23 to test the validity of existing descriptive protocols and parametric ecohydrological models.
24 The results showed that the VRD decreased with soil depth for the three plants and that it can
25 be effectively described with a negative exponential equation. Key VRD parameters, such as

26 the mean rooting depth, cross-sectional area at the root collar, and root biomass, were both site
 27 and species-specific but they were chiefly influenced by the attributes regulating the soil's
 28 water mass balance. The existing parametric ecohydrological models were not able to portray
 29 successfully the VRD of the studied alpine plants but we found a strong correlation between
 30 empirical and parametric VRD models that establish a clear direction for future research.
 31 Future work should address the influence of the snowpack characteristics and the length of the
 32 snow-free and frozen ground periods on the soil's ecohydrology and VRD in alpine
 33 ecosystems.

34

35 Keywords: root, model, ecohydrological, alpine, data mining

36

37 Abbreviations

38

α	Mean precipitation intensity over VSD	θ_{fc}	Soil moisture at field capacity
AI	Aridity index	θ_g	Gravimetric soil moisture content
ALR	Allometry ratio	θ_{wp}	Soil moisture at wilting point
Ar	Root cross-sectional area	ρ_{bk}	Soil's bulk density
Aro	Cross-sectional area at root collar	ρ_r	Root mass density
b	Mean rooting depth	Sa	Soil's sand content
Cl	Soil's clay content	Sk	Soil skeleton
CN	Concave topographic curvature	SOC	Soil organic carbon
CS	Plant's crown spread	Sp	Plant's aerial projected area
CX	Convex topographic curvature	Tbase	Optimum temperature for plant growth
Etp	Potential evapotranspiration	Tmn	Daily minimum air temperature
FL	Flat topographic curvature	Tmx	Daily maximum air temperature
GDD	Growing-degree day	VRD	Vertical root distribution
λ	Precipitation frequency over VSD	VSD	Vegetative season duration
Ma	Aboveground biomass	WAP	Water available to plants
Mr	Belowground biomass	z	Soil depth
n	Soil porosity		

39

40

41

42

43

44

45

46

47 1. Introduction

48

49 Knowledge of root systems of different vegetation types is essential for a better understanding
50 of biogeochemical processes occurring at the soil-plant-atmosphere continuum (Rodriguez-
51 Iturbe and Porporato, 2005). Despite relatively recent efforts in investigation and description
52 of plant root architecture (e.g., Waisel et al., 2002, Mickovski and Ennos 2003, Mickovski and
53 van Beek 2005), it remains largely unexplored for most plant species. A number of authors
54 have explored root system architecture of a large number of plants native to almost all
55 bioclimatic regions (e.g. Schenk and Jackson, 2005), and attempted prediction of rooting
56 depths through optimisation (van Wijk and Bouten, 2001; Kleidon, 2004) or inverse methods
57 (Zuo and Zhang, 2002). These approaches led to an increase in knowledge and understanding
58 of plant physiological processes such as water and nutrient uptake, resources competition, and
59 plant-soil interactions (Herbert et al., 2004; Laio et al., 2006, Preti et al., 2010; Gonzalez-
60 Ollauri and Mickovski, 2017a). Despite the efforts in the past decade, the comprehensive
61 understanding of the effect of soil and plant properties and climate conditions on root
62 architecture and morphology remains largely unknown.

63

64 Obtaining root information is time-consuming and methodologically challenging. The
65 investigation of root systems normally involves destructive and invasive sampling approaches
66 (Bhöm, 1979), followed by detailed description and measurement of specific root traits (Stokes
67 et al., 2009). However, for many environmental applications related to plant-soil interactions,
68 knowledge of the vertical root distribution (VRD) – i.e. the pattern in which root density
69 biomass is distributed along the soil profile - is perhaps the most important feature to know

70 because it can be used, for example, to estimate the degree of soil-root mechanical
71 reinforcement (Arnone et al., 2016; Gonzalez-Ollauri and Mickovski, 2016; Kokutse et al.,
72 2016), to estimate plant-water uptake (Jarvis, 1989; Laio, 2006; Shukla, 2014), or to gain
73 insight into the ability of vegetation to remove pollutants from the soil (Verma et al., 2006;
74 Gonzalez-Ollauri and Mickovski, 2018; Lucherini et al., 2020). For most of these applications,
75 VRD can be easily portrayed with asymptotic mathematical functions (Jackson et al., 1996),
76 which substantially simplify the process of describing the root system, as they normally require
77 few parameters related to the root system, such as the rooting depth or the cross-sectional area
78 at the root collar (Preti et al., 2010). However, standard and reproducible protocols to describe
79 VRD are still lacking.

80

81 The way in which roots distribute in the soil has been the scope of research for many decades
82 (e.g. Darwin, 1880; Laio et al., 2006). Previous research indicates that the root distribution in
83 the soil is mostly influenced by water availability to plants (i.e. hydrotropism; Tsutsumi et al.,
84 2003). This is relevant because it permits to connect VRD to climate and soil attributes
85 regulating the water cycle in the soil (e.g. soil porosity, soil organic matter, soil texture, etc;
86 Toth et al., 2015), and to set the basis for establishing cost-effective analytical approaches
87 describing VRD on the basis of few, easy-to-measure variables. As a result, and to the best of
88 our knowledge, two parametric, ecohydrological models predicting VRD have been developed
89 for arid or semi-arid (Laio et al., 2006; Preti et al., 2010) and for temperate-humid (Gonzalez-
90 Ollauri and Mickovski, 2016) ecosystems, respectively. These models incorporate plant-
91 specific attributes by considering the relative allocation of plant biomass between the above-
92 and belowground soil compartments (i.e. allometry; Cheng and Niklas. 2007) and by assuming
93 that the root system can take a known, simple geometrical shape, such as a cylinder, a cone, or
94 a hemisphere (e.g. Lynch, 1995; Kutschera and Lichtenegger, 1992; Kokutse et al., 2006). The

95 ability of these models to realistically portray VRD has been successfully tested for few
96 herbaceous (Gonzalez-Ollauri and Mickovski, 2016) and shrub species (Preti and Giadrossich,
97 2009; Preti et al., 2010), but their application to the wider pool of plants, in general, and to
98 woody plants (e.g. Preti et al., 2010; Tron et al., 2014; Tardio et al., 2016), in particular, needs
99 further validation. In addition, the robustness of the model conceptualisation and the
100 assumptions still need to be verified against primary data showing the influence of multiple
101 soil and plant attributes on VRD, which could help to identify potential model improvements
102 including application to climates with different ecohydrological features, such as tropical or
103 alpine.

104

105 Alpine ecosystems are normally found above the upper limit of tree growth in mountainous
106 areas. They are generally characterised by cold winter temperatures, precipitation in the form
107 of snow, and short snow-free periods (Freppaz et al., 2019) – all of which tend to limit the
108 duration of the vegetative season. As a result, alpine vegetation, which mostly comprises low-
109 growing herbaceous perennial plants, tends to be sparse and endemic to these ecosystems, or
110 it may have evolved to withstand the environmental stress related to alpine climates (Germino,
111 2014). In addition, the growth and development of alpine plants is also constrained by the low
112 availability of nutrients in the soil, particularly nitrogen (e.g. Freppaz et al., 2019; Zong et al.,
113 2020). Still, alpine vegetation may play a crucial role in cycling carbon and nutrients in alpine
114 ecosystems (e.g. Iversen et al., 2014), or in protecting the soil against shallow landslides and
115 erosion (Preti, 2013; Burylo et al., 2014; Gonzalez-Ollauri and Mickovski, 2017b), where
116 poorly developed soils subjected to freezing are prone to soil mass wasting processes (e.g.
117 Hudek et al., 2017a). Yet, knowledge of the root systems in alpine plants is scarce (e.g. Iversen
118 et al., 2014) and only few studies have attempted addressing this knowledge gap (e.g. Pohl et
119 al., 2011; Burylo et al., 2014; Hudek et al., 2017b).

120

121 The aim of this study is to describe the VRD of three dominant alpine plants on the basis of
122 simple and easy-to-measure climate, soil, and plant attributes in order to test existing
123 descriptive protocols and parametric ecohydrological models. The objectives of the study
124 include (i) selection and characterisation of three alpine sites in terms of climate and soil
125 attributes, (ii) sampling above- and below-ground plant parts of three dominant pioneer plant
126 species from the three study locations to retrieve relevant plant information and to describe the
127 VRD, (iii) investigation of the influence of evaluated soil and plant attributes on key VRD
128 parameters, and (iv) testing the predictive capacity of an existing parametric ecohydrological
129 model for VRD using pedo-climatic and plant attributes.

130

131 2. Materials and Methods

132

133 2.1. Study area

134

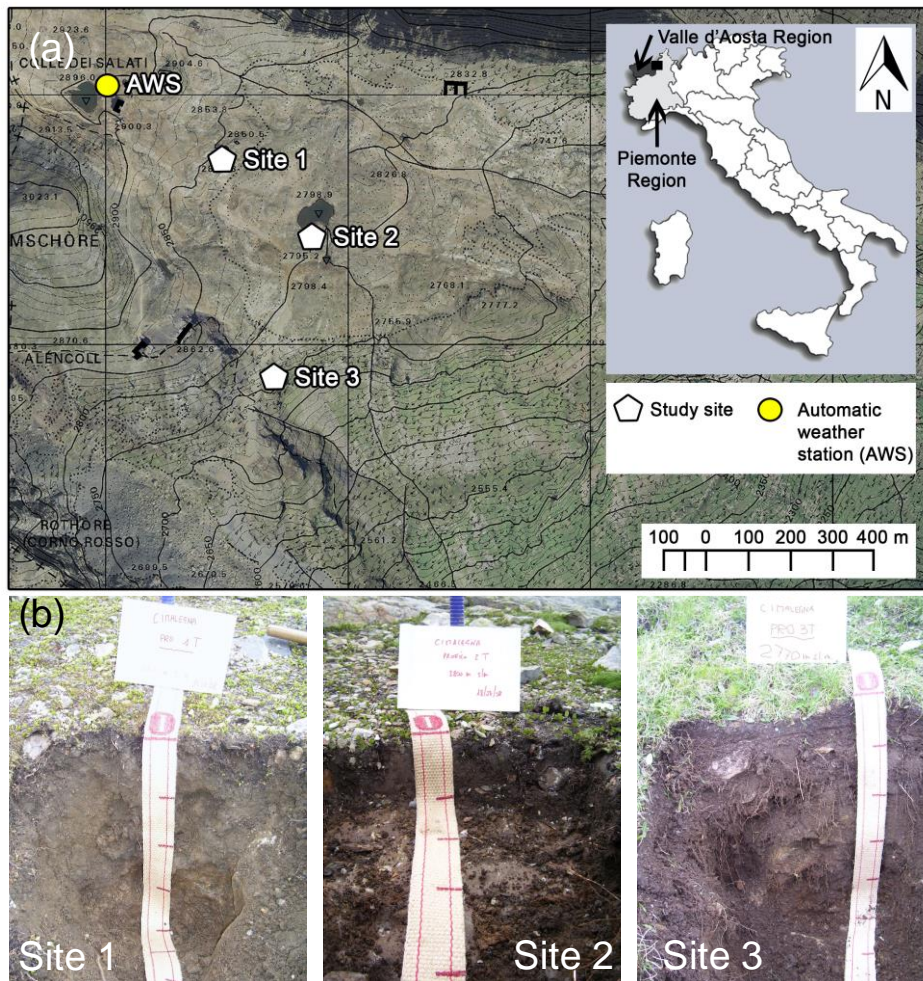
135 The study area is located adjacent to Monte Rosa massif (4634 m above sea level; a.s.l.), within
136 the Long-Term Ecological Research (LTER) site Angelo Mosso Institute, Valle d'Aosta
137 Region, Northwest Italy (Fig. 1a). The climate in the study area is Alpine (ET; Köppen, 1884),
138 characterised by a mean annual air temperature of -2.5°C , a cumulative annual snowfall of 8.50
139 m, and a mean annual rainfall of 350 mm. The snowpack generally develops in late October -
140 early November and lasts until the onset of snowmelt in late May – early June. Soil temperature
141 and meteorological parameters such as air temperature, rainfall during the snow-free season,
142 and snowfall have been continuously recorded with a 1-minute resolution in the study area
143 since 2005 using one Automatic Weather Station (AWS) located at 2901 m a.s.l. (Fig. 1;
144 Comando Truppe Alpine - Servizio Meteomont).

145

146 Three, high-altitude study sites located in the upper part of a glacier valley were selected within
147 the study area (Fig. 1a). The sites were located at different elevations and had distinct
148 underlying soil types -i.e. Site 1: 2840 m a.s.l on Dystric Leptic Regosol; Site 2: 2795 m on
149 Dystric Lithic Leptosol ; Site 3: 2770 m on Haplic Umbrisol (IUSS Working Group WRB,
150 2015). Sites 1 and 2 (Figs.1b and 1c) are characterised by relatively flat topographies. The
151 dominant vegetation at these sites comprises nival plant species of perennial grasses (*Poa laxa*,
152 *Poa alpina*), together with other herbaceous species such as forbs (*Leucanthemopsis alpina*,
153 *Gnaphalium supinum*), cushion plants (*Minuartia sedoides*) and dwarf, woody plants that can
154 tolerate long-lasting snow cover (*Salix herbacea*, *Loiseleuria procumbens*). The topography of
155 Site 3 is rougher and the vegetation cover denser than at sites 1 and 2 (Fig. 1a). Alpine
156 grasslands dominate Site 3 with the most characteristic plant species being *Carex curvula* and
157 *Euphorbia minima* (Freppaz et al., 2019; Lonati et al., unpublished data).

158

159



160

161 *Figure 1 a) Locations of the study sites (1-3) and b) characteristic soil profiles for site 1, 2 and 3.*

162

163 2.2.Climatic attributes

164

165 We measured four climatic attributes reported to influence plant growth and root development
 166 (e.g. Preti et al., 2010; Gonzalez-Ollauri and Mickovski, 2016), and which are nested in the
 167 parametric, ecohydrological VRD model to be tested herein (Section 2.6; Table 1). To this end,
 168 we examined daily meteorological records collected with one AWS between 2005 and 2019
 169 (Fig. 1a), which we assumed to be representative for the three study sites. The vegetative season
 170 duration (VSD) was defined using the heuristic growing-degree days (GDD; Eq.8) approach
 171 (e.g. McMaster and Wilhelm, 1997), which is a measure of the daily heat accumulation to

172 predict plant development and phenology. We assumed that the vegetative season begun once
173 the cumulative GDD reached 200°C (Eq.8; Table 1), and that it ended when daily mean soil
174 temperature was below 4°C (i.e. root growth is inhibited under 4°C; e.g. Alvarez-Uria and
175 Körner, 2007). We also assumed 5°C as the optimum soil temperature for plant growth (T_{base} ;
176 Eq.8; Table 1). We then calculated the aridity index (AI) of the study site as the ratio of the
177 total potential evapotranspiration to the total precipitation (Eq. 9; Table 1; Greve et al., 2019)
178 over the vegetative season. The total precipitation was considered as the sum of rainfall and
179 snowfall (i.e. snow water equivalent) recorded during the vegetative season of each examined
180 year. The total potential evapotranspiration over the vegetative season, which is in turn nested
181 in the VRD model (Eq.4; Table 1), was calculated with the Priestly and Taylor (1972) equation
182 (Eq. 10; Table 1). Subsequently, we estimated the mean precipitation depth (α , mm event⁻¹)
183 and the frequency of precipitation events (λ) during the vegetative season (Laio et al., 2006;
184 Preti et al., 2010). We calculated α as the ratio of the total precipitation to the number of
185 precipitation events (i.e. days with precipitation > 0.2 mm) during the vegetative season
186 averaged for the studied time period comprised between 2005 and 2019. Rainfall lost to surface
187 runoff was assumed to be negligible in our study area (e.g. Tron et al., 2014). We calculated λ
188 as the ratio of the number of precipitation events to the total vegetative season duration
189 averaged for the studied period.

190

191 2.3. Soil attributes

192

193 The slope gradient and aspect were measured manually with a hand-held inclinometer and with
194 a compass, respectively, at locations adjacent to each sampled plant individual (Section 2.4).
195 The terrain curvature of each sampling location was visually described as either concave (CN),
196 convex (CX) or flat (FL) (e.g. Gonzalez-Ollauri and Mickovski, 2017c). Undisturbed soil

197 samples (N=36) from the topsoil (0 mm - 100 mm below ground level; b.g.l) were collected at
198 the same locations where plants were sampled using a soil core sampler. These samples were
199 used to determine the soil bulk density (ρ_{bk} ; g cm⁻³), soil porosity (n) and gravimetric moisture
200 content (θ_g ; %) following standard methods (Head, 1980). The soil organic carbon (SOC ; %)
201 and pH were determined using a portion of the collected soil materials, which was air-dried for
202 168 h and sieved through a 2 mm opening sieve. SOC was determined using a C/H/N analyser
203 (Elementar Vario EL) while soil pH was determined in soil–water suspension (soil: water =
204 1:2.5) following the slurry method (ASTM, 1995) and using a pH electrode (Fisher Scientific
205 Accumet Basic AB15). Additional soil materials in form of bulk samples of 4kg-5kg were
206 collected with a shovel from the topsoil (0 mm – 300 mm b.g.l) at three representative locations
207 per study site (N=9). These representative sampling locations, which were assumed to capture
208 the main soil features within a study site, were within the area range covered by plant sampling,
209 and were less than 5 m away from any given plant individual sampled in this study. The soil
210 samples were stored in heavy-duty PVC bags and transported to the laboratory where they were
211 mixed per study site (N=3) prior to further analysis. The particle size distribution (PSD) of the
212 collected soil materials was determined through the dry sieving and the hydrometer methods
213 for the coarse (i.e. gravel and sand) and fines (i.e. silt and clay) fractions, respectively (Head,
214 1980). The soil skeleton (i.e. percentage of rock fragments in the soil sample; Sk ; %) was
215 determined through dry sieving (Head, 1980). Soil moisture content at field capacity (θ_{fc} ; %)
216 and wilting point (θ_{wp} ; %) were estimated through pedotransfer functions (Eqs. 11 and 12;
217 Table 1; Toth et al., 2015), which are nested in the VRD model and use PSD, n , and SOC as
218 inputs.

219

220 2.4. Plant species, plant attributes and vertical root distribution

221

222 We selected three dominant, characteristic plant species for the study from sites 1, 2, and 3
223 (Fig.1):

224 (i) dwarf eyebright (*Euphrasia minima* Jacq.), an annual, facultative root hemiparasite
225 (Matthies, 1998; Fig. 2a) with erect stems reaching up to 150 mm, which grows in
226 humid mountainous habitats between 950-3000 m a.s.l. (Asturnauta, 2020)

227 (ii) alpine chrysanthemum (*Leucanthemopsis alpina* L.), a perennial, herbaceous plant
228 belonging to the daisy family and specific to high alpine elevations, growing
229 between 1800-3500 m a.s.l. It can be an early coloniser after the retreat of glaciers,
230 being generally small in size (< 200 mm in height) with a root system characterised
231 by horizontal rhizomes (ukwildflowers.com, 2020; Fig. 2b).

232 (iii) alpine bluegrass (*Poa alpina* L.), a subartic-alpine meadow tufted grass found in
233 moist to dry limestone and in basaltic rock crevices and exposed heathlands. It is a
234 pseudoviviparous, apomictic, and fast germinating plant (Pierce et al., 2000) that
235 can reach up to 400 mm in height, normally has narrow leaves (2-4 mm), and its
236 inflorescence is pyramidal, twice as tall as wide; it also has an adventitious root
237 system that arises extra-vaginally through the leaf-sheaths at the base of the plant
238 (Pierce et al., 2000; Fig. 2c).



239

240 *Figure 2. Selected root systems of (a) Euphrasia minima (b) Leucanthemopsis alpina (c) Poa alpina.*

241 Plant sampling was undertaken at the height of the growing season when four individuals per
 242 plant species were sampled at random locations within each study site (N=36; Fig. 1). The
 243 projection area of the aerial plant parts (Sp ; cm^2 ; total plant aboveground area projected on the
 244 ground, assuming a plant crown with a circular shape) and average crown spread (CS ; cm ;
 245 mean spread diameter of the aboveground plant parts) were measured for each sampled
 246 individual with a meter tape following the Spokes distance method (Blozan, 2006). Each plant
 247 individual was excavated by hand before being clipped with scissors above the root collar (Fig.
 248 3) to separate the above from the belowground part. The aboveground plant materials were
 249 oven-dried at 60°C until constant mass to measure the aboveground biomass (Ma ; g) of each
 250 sampled individual. The belowground parts were cleaned with a water jet to separate soil
 251 particles attached to the root system prior to being air-dried for 2 h for describing the vertical
 252 root distribution (VRD).

253

254 VRD was measured manually as the total cross-sectional root area at a given soil depth (Fig.
 255 3) for each sampled plant before being averaged per plant species and study site. Using a
 256 permanent marker and a ruler, marks were drawn on the root systems at equal length intervals

257 ranging from 5 to 20 mm and starting from the root collar (Fig. 3) to visualise the assumed
258 root-soil intersection planes (Fig. 3). The diameter of all the roots intersecting each plane was
259 measured with Vernier callipers, and their cross-sectional area ($A_r(z)$; mm²) was calculated
260 with Eqs. 1 and 2 (Table 1; Fig. 3), assuming all roots had circular cross-section when crossing
261 a given intersection plane (Fig. 3). Subsequently, A_r was averaged per intersection plane and
262 per plant species for a given sampling site. Then, a nonlinear least squares (nls) exponential
263 model of the form $y = ae^{-x/b}$, where y is the dependent variable (i.e. root cross-sectional area;
264 A_r), x is the independent variable (i.e. soil depth), and a and b are fitting parameters (Eq.3;
265 Table 1) was fitted to the measured data resulting from the previous step. With this approach
266 and, for modelling purposes, it was assumed that the root biomass is distributed in the soil
267 following a cone shape volume (Fig. 3b; Preti et al., 2010; Gonzalez-Ollauri and Mickovski,
268 2016; see Supplementary Material) in which the total rooting depth (i.e. soil depth at which 95
269 % of roots are found; $3xb$; mm; Laio et al., 2006) was the cone's height and the cross-sectional
270 area of the root collar (A_{ro} ; mm²) the cone's basal area (Fig. 3b). Accordingly, the rooting
271 depth (b ; mm) was quantified as 1/3 of the longitudinal distance between the root collar and
272 the tip of the root system of each studied individual (Laio et al., 2006). It must be borne in
273 mind that with the former cone-shape-volume approach (Fig. 3b), we are not trying to capture
274 the shape of the root system *per se* (Fig. 2; e.g. Köstler et al., 1968) but to provide a generic
275 basis to model the widely-observed decrease in root biomass with soil depth (e.g. Schenk,
276 2005; see Supplementary Material). Finally, the root materials were oven-dried at 60°C until
277 constant mass to measure the root biomass (M_r ; g) and the allometry ratio (ALR) as the quotient
278 between M_r and M_a .

279

280 Table 1. List of equations used in this study. Arid and humid ecosystems are defined on the basis of the aridity index (AI) over the growing season -i.e. $AI < 1$: arid; $AI > 1$: humid; ppu: parts-per
 281 unit. VS: vegetative season.

282

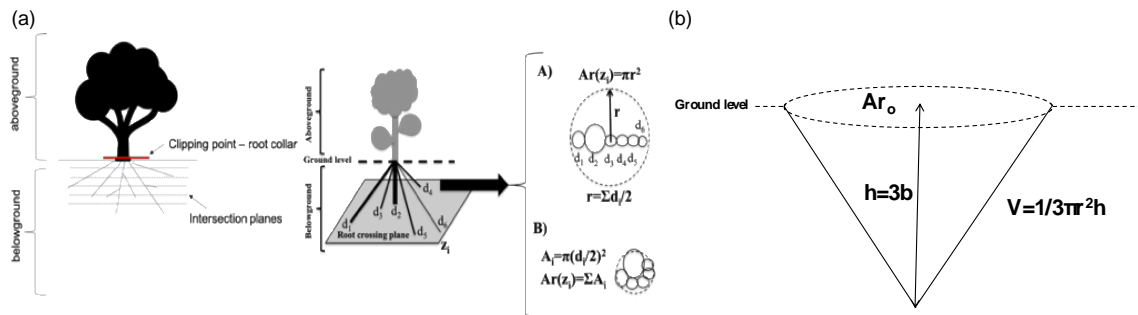
Definition	Equation	No	Parameters	Units	Source
Cross-sectional area of the i^{th} root at a given intersection plane	$A_i = \pi (dx/2)^2$	Eq. 1	A_i : cross-sectional area of the i^{th} root at a given intersection plane dx : root diameter	mm ² mm	Gonzalez-Ollauri and Mickovski (2016)
Root cross-sectional area at a given intersection plane	$Ar(z_i) = \Sigma A_i$	Eq.2	$Ar(z_i)$: cross-sectional area of all roots crossing a given intersection plane	mm ²	Gonzalez-Ollauri and Mickovski (2016)
Vertical root distribution (VRD)	$Ar(z) = Aro \cdot e^{-\frac{z}{b}}$	Eq. 3	$Ar(z)$: cross-sectional area of all roots along the soil profile Aro : cross-sectional area of the plant stem above the root collar b : mean rooting depth z : soil depth	mm ² mm ² mm mm	Preti et al. (2010)
Mean rooting depth in arid and semi-arid ecosystems	$b = \frac{\alpha}{n(\theta_{fc} - \theta_{wp})(1 - \frac{\lambda\alpha}{Etp})}$	Eq. 4	α : mean precipitation intensity per event over the growing season n : soil porosity θ_{fc} : volumetric soil moisture content at field capacity	mm event ⁻¹ ppu ppu	Laio et al. (2006)

			<p>θ_{wp}: volumetric soil moisture content at wilting point</p> <p>λ: frequency of precipitation events over the growing season</p> <p>Etp: total potential evapotranspiration over the growing season</p>	<p>ppu</p> <p>events</p> <p>mm</p>	
Mean rooting depth in humid ecosystems	$b = \frac{\alpha}{n(\theta_{fc} - \theta_{wp})}$	Eq. 5			Gonzalez-Ollauri and Mickovski (2016)
Water available to plants in the soil	$WAP = \theta_{fc} - \theta_{wp}$	Eq. 6	WAP : water available to plants	ppu	
Area at the root collar	$Aro = \frac{Mr}{b \rho_r}$	Eq. 7	<p>Aro: cross-sectional area of the plant stem above the root collar</p> <p>Mr: plant belowground biomass</p> <p>ρ_r: root mass density</p>	<p>mm²</p> <p>g</p> <p>g mm⁻³</p>	Preti et al. (2010)
Growing-degree day	$GDDi = \frac{T_{mx} - T_{mn}}{2} - T_{base}$	Eq.8	<p>T_{mx}: daily maximum air temperature</p> <p>T_{mn}: daily minimum air temperature</p>	°C	McMaster and Wilhelm (1997)

	$\begin{cases} \sum_{i=1}^n GDDi \geq 200^{\circ}\text{C.} & VS \text{ start} \\ T_{soil} \leq 4^{\circ}\text{C} & VS \text{ end} \end{cases}$		<i>Tbase</i> : optimum daily mean temperature for plant growth <i>i</i> : i th day <i>Tsoil</i> : daily mean soil temperature	$^{\circ}\text{C}$ $^{\circ}\text{C}$	
Aridity index	$AI = \frac{Etp}{PCP}$	Eq. 9	<i>PCP</i> : total precipitation over the growing season	mm	Greve et al. (2019)
Potential evapotranspiration	$Etp = 0.00128 \frac{Rnl \Delta}{58.3 \Delta + \gamma}$	Eq. 10	<i>Rnl</i> : net solar radiation Δ : slope of saturation vapour pressure γ : psychrometric constant	MJ m ⁻² day ⁻¹ kPa $^{\circ}\text{C}$ kPa $^{\circ}\text{C}$	Priestly and Taylor (1972)
Soil moisture at field capacity	$\theta_{fc} = \theta_{33} + 1.23\theta_{33}^2 - 0.374\theta_{33} - 0.015$ $\theta_{33} = -0.251Sa + 0.195Cl + 0.011SOC$ $+ 0.006Sa.SOC$ $- 0.027Cl.SOC + 0.452Sa.Cl$ $+ 0.299$	Eq. 11	θ_{33} : soil moisture at -33 kPa of matric suction <i>Sa</i> : sand content in the soil <i>Cl</i> : clay content in the soil <i>SOC</i> : soil organic carbon	ppu ppu ppu ppu	Toth et al. (2015)
Soil moisture at wilting point	$\theta_{wp} = \theta_{1500} + 0.14\theta_{1500} - 0.02$ $\theta_{1500} = -0.024Sa + 0.487Cl + 0.006SOC$ $+ 0.005Sa.SOC$ $- 0.013Cl.SOC + 0.068Sa.Cl$ $+ 0.031$	Eq. 12	θ_{1500} : soil moisture at -1500 kPa of matric suction	ppu	Toth et al. (2015)

284

285



286

287

288

289

290

291

292

293

Figure 3. (a) Illustration of the methodological approach followed to separate aboveground and belowground plant parts and to describe vertical root distribution (VRD) for the studied plant species. Approach B was followed to describe the cross-sectional area of all roots at a given crossing plane ($A_r(z)$), as it does not overestimate the root cross-sectional area compared to approach A. r stands for the rooting radius and d for the diameter of i th root at a given crossing plane. (b) VRD was modelled as a cone with base's area A_{r_0} (i.e. root collar area; mm^2) and height $3b$, being b the mean rooting depth (mm) and $3b$ the soil depth at which 95% of the roots are found (Laio et al., 2006). V stands for the cone volume and h for the cone height. See mathematical formulation in Supplementary Material.

294

295

2.5. Relationship between soil and plant attributes with key VRD parameters

296

297

298

299

300

301

302

303

304

We investigated the relationship between the studied soil (Section 2.3) and plant attributes (Section 2.4) with the relevant/key parameters used to portray VRD (A_{r_0} : cross-sectional area of the root collar, and b : mean rooting depth) through a data mining workflow (Supplementary Material – Fig. S1) which was built using the statistical language R v5.5.1 (R Core team, 2018). We also included plant belowground biomass (Mr) in the analysis, as Mr will ultimately limit the extent of VRD (Gonzalez-Ollauri and Mickovski, 2016). This workflow was used to accomplish three objectives: (i) to evaluate the ability to predict relevant VRD parameters using the investigated soil and plant attributes as predictors, (ii) to evaluate the importance of

305 each plant and soil predictor on the relevant VRD parameters, and (iii) to evaluate predictor-
306 response dependency - i.e. how the response variable changes following predictor changes.

307

308 To accomplish objective (i), 100 random forest models (RF; Breiman, 2001) were fitted with
309 1000 regression trees each, using the R package “randomForest” (Liaw and Wiener, 2020).
310 Only uncorrelated attributes to the VRD parameters were considered to fit RF models. Each
311 RF model was cross-validated with a bootstrapping method without replacement (e.g.
312 Gonzalez-Ollauri et al., 2020) and through the evaluation of the coefficient of determination
313 (R^2), root mean square error (RMSE) and variance explained (VExp) following the least-
314 squares method (Fuller, 1987). The pool of cross-validation coefficients retrieved from
315 implementing the data mining workflow was examined by plotting their corresponding
316 probability density functions (Appendix A).

317

318 To accomplish objective (ii), the importance of each plant and soil attribute on the response
319 variables (i.e. key VRD parameters) was examined on the basis of permutation tests using the
320 R package “caret” (Khun et al., 2018), which measures attribute importance by observing
321 model performance when each predictor is randomly dropped out from fitting a RF model
322 during the training step (e.g. Strobl et al., 2008).

323

324 To achieve objective (iii), we examined the Partial Dependence Plots (PDPs; Hastie et al.,
325 2009) retrieved from using the R package “pdp” (Greenwell, 2017). PDPs were retrieved to
326 show whether the interaction between a target VRD parameter and a target plant and soil
327 attribute was linear, monotonic, or more complex in the fitted RF models, representing how a
328 given attribute influenced the prediction on average for a given VRD parameter. The R script
329 used to implement the data mining workflow described above is provided in Appendix C.

330
331
332
333
334
335
336
337
338
339
340
341
342
343
344
345
346
347
348
349
350
351
352
353
354

2.6. Empirical vs. parametric, ecohydrological model for vertical root distribution

We tested the predictive capacity of an existing parametric ecohydrological model for vertical root distribution (Eqs. 4-5, Table 1; Laio et al. 2006; Preti et al., 2010; Gonzalez-Ollauri and Mickovski, 2016) against the empirical VRD model fitted to the measured data described in Section 2.4. The parametric ecohydrological VRD model was firstly developed for arid and semi-arid ecosystems by Laio et al. (2006) and extended by Preti et al. (2010), and then adapted to temperate-humid climates by Gonzalez-Ollauri and Mickovski (2016). This model estimates the mean rooting depth (b ; Eqs. 4 and 5; Table 1) on the basis of pedo-climatic parameters (i.e. α : mean precipitation depth during the growing season; λ : frequency of precipitation events; Etp : potential evapotranspiration; Section 2.2) and of the product between soil porosity (n) and the water available to plants in the soil (WAP ; Eq. 6; Table 1), function of the difference between the volumetric soil moisture content at field capacity (θ_{fc}) and at wilting point (θ_{wp}). Different equations for b must be considered depending on whether the aridity index (AI ; Eq. 8) is greater than 1 (i.e. arid climate; Eq. 4; Preti et al., 2010) or lower than 1 (i.e. humid climate; Eq.5; Gonzalez-Ollauri and Mickovski, 2016). VRD is then modelled with a negative exponential equation (Eq. 5; Table 1) using b , the cross-sectional area at the root collar (A_{ro}) and the soil depth (z ; mm) as inputs, assuming that the probability density function for the daily rainfall intensity at the study site is exponentially distributed (Laio et al., 2006). The cross-sectional area at the root collar (A_{ro}) is estimated using plant-specific information and the rooting depth under the assumption that the distribution of root biomass along the soil profile can be portrayed with a conical-shape-volume (Fig. 3b; Section 2.4; Eq. 6; Table 1; supplementary material). In addition, we assumed that the portion of soil explored by roots was uniform and isotropic.

355

356 The outcomes from the parametric, ecohydrological and the empirical VRD models were
357 compared in the light of the outputs for the root cross-sectional area (A_r) of all roots along the
358 soil profile. To do so, A_r was firstly retrieved for soil depths of 0 mm - 100 mm using the
359 parametric ecohydrological and empirical VRD models (Section 2.4), respectively. Then, the
360 two A_r datasets were log-transformed and plotted together to graphically evaluate the
361 mathematical relationship between the two models. Subsequently, a linear regression model
362 was fitted between the two retrieved, log-transformed A_r datasets in R v3.5.1. Additionally,
363 the correlation between the linear fitting parameters and the studied plant and soil attributes
364 was examined by estimating pairwise Pearson's correlation coefficients.

365

366 2.7. Statistical analysis

367

368 Normality checks were undertaken for every studied soil and plant attribute with the Shapiro
369 Wilk test. Soil and plant attributes were aggregated into plant species and study site,
370 respectively, for statistical analysis. Statistical differences in plant attributes between plant
371 species and investigation site were evaluated with the non-parametric Kruskal Wallis (χ^2) test,
372 as plant attributes did not follow a normal distribution. Where statistically significant
373 differences were encountered, plant attribute's differences between two plant species were
374 evaluated with the non-parametric Wilcoxon (W) test. Statistical differences in soil attributes
375 between plant species and investigation site were evaluated with one-way ANOVA (F) and
376 Kruskal Wallis (χ^2) tests for normal and non-normal distributed variables, respectively.
377 Vertical root distribution (VRD) differences between investigated sites were evaluated per
378 plant species with the Kruskal Wallis (χ^2) test, as VRD did not follow a normal distribution.
379 Where statistically significant differences were encountered, the differences within the plant

380 species were evaluated with the non-parametric Wilcoxon (W) test. VRD differences between
381 plant species for a given investigation site were examined with the same approach indicated
382 before. Statistical differences between the importance of the attributes used as predictors for
383 the selected VRD parameters were also evaluated with the Kruskal Wallis test. The statistical
384 relationship between the studied plant and soil attributes was evaluated with the pair-wise
385 Pearson's correlation test and interpreted on the basis of the resulting correlogram plot. All
386 statistical tests were carried out at the 95 % and 99 % confidence level using the 'base' package
387 embeddedw in the statistical computing software R v3.5.1 (R Core Team, 2018).

388

389 3. Results

390

391 3.1. Climate attributes

392

393 The growing season duration for the period 2005-2019 was on average 50 ± 18 days long,
394 generally starting in early July and ending in early September. The aridity index of the study
395 site during the snow-free period was 0.91 ± 0.2 , indicating that the temperate-humid,
396 ecohydrological VRD model (Eq.5; Table 1) must be implemented for the study area. The
397 mean precipitation depth per event during the growing season (α) was 6.68 ± 2.33 mm, the
398 frequency of precipitation events (λ) was 0.56 ± 0.05 , and the total potential evapotranspiration
399 (E_{tp}) during the vegetative season was 68.8 ± 2.1 mm.

400

401 3.2. Soil attributes

402

403 The examined soil attributes (Table 2) differed significantly between the investigated study
404 sites. Site 3 had a substantially higher slope gradient ($\chi^2: 18.2$ df:2 $p < 0.01$), it was consistently

405 concave in terms of the terrain curvature, and it had a more South-facing aspect than Sites 1
406 and 2. In addition, Site 3 had a significantly higher soil moisture (F:65.89 df:1 p<0.01), soil
407 organic carbon (F:45.3 df:1 p<0.01), and proportion of fine soil materials (χ^2 :35 df:2 p<0.01)
408 than Sites 1 and 2, while having a substantially lower bulk density (χ^2 :20.2 df:2 p<0.01), soil
409 skeleton (χ^2 :35 df:2 p<0.01), and coarse soil materials (χ^2 :35 df:2 p<0.01) than the other two

410 Table 2. Soil attributes investigated in this study averaged per plant species and per sampling site \pm standard deviation. θ_g : gravimetric moisture content; ρ_{bk} : dry bulk density; n : soil porosity;
 411 SOC: soil organic carbon; Sk: soil skeleton.

		Slope (°)	Curvature	Aspect	θ_g (%)	ρ_{bk} (g cm ⁻³)	n	SOC (%)	pH	Sk (%)
Plant species	<i>Euphrasia minima</i>	8.42 \pm 8.7	convex	145.42 \pm 22.8	29.20 \pm 11.4	1.18 \pm 0.2	0.56 \pm 0.1	7.70 \pm 2.6	4.50 \pm 0.1	20.70 \pm 7.2
	<i>Leucanthemopsis alpina</i>	8.42 \pm 6.3	flat/convex	145 \pm 25.3	27.46 \pm 9.3	1.24 \pm 0.2	0.53 \pm 0.1	6.59 \pm 1.4	4.50 \pm 0.1	20.70 \pm 7.2
	<i>Poa alpina</i>	11.50 \pm 7.3	flat/convex	152.08 \pm 18.8	27.43 \pm 9.2	1.20 \pm 0.2	0.55 \pm 0.1	7.83 \pm 2.6	4.50 \pm 0.1	20.70 \pm 7.2
Sampling site	Site 1	6.92 \pm 4.5	flat/convex	133.50 \pm 11.1	19.44 \pm 7.1	1.37 \pm 0.2	0.48 \pm 0.1	5.52 \pm 1.4	4.60 \pm 0.0	16.30 \pm 0.0
	Site 2	4.33 \pm 2.1	convex	135.5 \pm 9.81	26.05 \pm 4.0	1.26 \pm 0.1	0.52 \pm 0.0	6.96 \pm 1.4	4.40 \pm 0.0	30.40 \pm 0.0
	Site 3	17.08 \pm 7.3	concave	173.5 \pm 14.9	38.60 \pm 5.5	0.98 \pm 0.2	0.63 \pm 0.1	9.64 \pm 1.6	4.50 \pm 0.0	15.40 \pm 0.0

412

413

414

415

416 Table 2 Cont. Soil attributes investigated in this study averaged per plant species and per sampling site \pm standard deviation. θ_{fc} : volumetric soil moisture content at field capacity; θ_{wp} :
 417 volumetric soil moisture content at wilting point.

		Clay (%)	Fine silt (%)	Coarse silt (%)	Fine sand (%)	Coarse sand (%)	θ_{fc} (%)	θ_{wp} (%)
Plant species	<i>Euphrasia minima</i>	1.40 \pm 0.34	5.67 \pm 1.11	11.30 \pm 3.33	50.73 \pm 3.64	30.87 \pm 2.15	27.851 \pm 0.3	1.56 \pm 0.04
	<i>Leucanthemopsis alpina</i>	1.40 \pm 0.34	5.67 \pm 1.11	11.30 \pm 3.33	50.73 \pm 3.64	30.87 \pm 2.15	28.33 \pm 0.2	2.01 \pm 0.10
	<i>Poa alpina</i>	1.40 \pm 0.34	5.67 \pm 1.11	11.30 \pm 3.33	50.73 \pm 3.64	30.87 \pm 2.15	29.18 \pm 0.4	3.09 \pm 0.20
Sampling sites	Site 1	1.00 \pm 0.0	4.30 \pm 0.0	9.20 \pm 0.0	52.30 \pm 0.0	33.20 \pm 0.0	28.78 \pm 0.7	2.37 \pm 0.9
	Site 2	1.40 \pm 0.0	5.80 \pm 0.0	15.80 \pm 0.0	45.90 \pm 0.0	31.20 \pm 0.0	28.10 \pm 0.6	2.20 \pm 0.7
	Site 3	1.80 \pm 0.0	6.90 \pm 0.0	8.90 \pm 0.0	54.00 \pm 0.0	28.20 \pm 0.0	28.23 \pm 0.9	2.16 \pm 0.7

418

419 investigated sites (Table 2). However, significant differences for the investigated soil attributes
420 were not detected between the three studied plant species (Table 2; $F:1.1$ $df:2$ $p=0.34$). The
421 available water to plants in the soil (Eq. 6, Table 1) was on average of 26.13 ± 0.3 %.

422

423 3.3.Plant attributes

424

425 The evaluated plant attributes (Table 3) were statistically different between the three studied
426 plant species. In particular, *Poa alpina* individuals had a substantially larger crown spread (CS;
427 $\chi^2:26.7$ $df:2$ $p<0.01$), plant projected area (*Sp*; $\chi^2:26.7$ $df:2$ $p<0.01$), cross-sectional area at the
428 root collar (*Aro*; $\chi^2:27.1$ $df:2$ $p<0.01$), aboveground biomass (*Ma*; $\chi^2:26.4$ $df:2$ $p<0.01$), and
429 root biomass (*Mr*; $\chi^2:29.3$ $df:2$ $p<0.01$) than those of the other two studied species (Table 3).
430 However, the measured mean rooting depth (*b*) was not statistically different between the three
431 studied plant species (Table 3; $\chi^2:0.6$ $df:2$ $p=0.76$). On other hand, the three investigated study
432 sites did not present statistical differences in terms of the evaluated plant attributes ($\chi^2:0.3$ $df:2$
433 $p=0.85$) with the exception of the observed *b*, which was significantly higher in Site 3 than in
434 Sites 1 and 2 (Table 3; $\chi^2:26.7$ $df:2$ $p<0.01$).

435

436 3.4. Vertical root distribution

437

438 The measured vertical root distribution (VRD) decreased exponentially with soil depth for the
439 three studied plant species and at the three study sites (Fig 5). As a result, negative exponential
440 models (Eq. 3. Table 1) were successfully fitted to the observed data (i.e. empirical model)
441 with high goodness of fit ($R^2>0.9$) in all cases. The model fitting parameters (Table 4) did not
442 differ statistically from the measured VRD parameters ($b:W=49$

443
444

Table 3. Plant attributes investigated in this study averaged per plant species and per sampling site \pm standard deviation . CS: crown spread; Sp: plant's aerial projected area; Aro: root collar area; b: mean rooting depth; Ma: aboveground biomass; Mr: root biomass; ALR: allometry ratio -i.e. Mr/Ma.

		CS (cm)	Sp (cm ²)	Aro (mm ²)	b (mm)	Ma (mg)	Mr (mg)	ALR
Plant species	<i>Euphrasia minima</i>	1.60 \pm 1.4	3.44 \pm 7.9	0.17 \pm 0.1	15.00 \pm 10.9	13.38 \pm 12.1	1.08 \pm 1.1	0.12 \pm 0.2
	<i>Leucanthemopsis alpina</i>	3.84 \pm 0.8	12.09 \pm 4.9	0.38 \pm 0.1	14.44 \pm 10.9	85.43 \pm 40.8	62.12 \pm 21.0	0.82 \pm 0.4
	<i>Poa alpina</i>	8.01 \pm 3.0	56.90 \pm 45.7	1.15 \pm 0.7	15.83 \pm 8.1	226.42 \pm 162.4	379.07 \pm 366.3	1.82 \pm 1.2
Sampling sites	Site 1	4.06 \pm 3.3	20.99 \pm 31.4	0.72 \pm 0.9	4.72 \pm 1.9	100.10 \pm 132.3	189.71 \pm 371.1	1.09 \pm 1.1
	Site 2	3.90 \pm 2.2	15.49 \pm 13.8	0.45 \pm 0.4	16.67 \pm 7.8	133.03 \pm 173.3	158.17 \pm 274.4	0.95 \pm 1.1
	Site 3	5.49 \pm 4.1	35.94 \pm 50.5	0.52 \pm 0.5	23.89 \pm 6.0	92.11 \pm 72.5	94.39 \pm 142.9	0.71 \pm 0.9

445

446
447
448

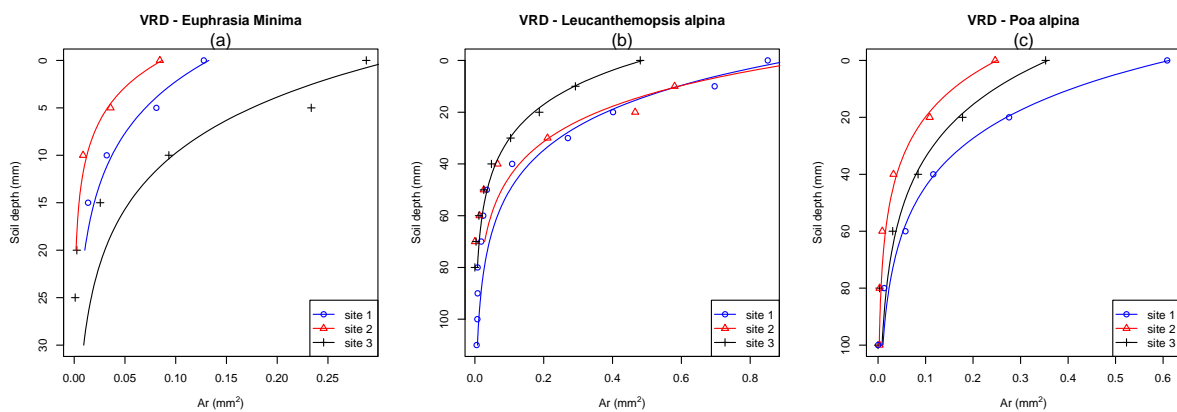
Table 24. Vertical root distribution (VRD) parameters measured, retrieved through fitting nls exponential models to the measured data -i.e. empirical VRD model (+), and predicted with the parametric, ecohydrological VRD model (++) per plant species and sampling site. b: mean rooting depth; Aro: cross-sectional area at the root collar.

Plant species	Site 1						Site 2						Site 3					
	b (mm)	b ⁺ (mm)	b ⁺⁺ (mm)	Aro (mm ²)	Aro ⁺ (mm ²)	Aro ⁺⁺ (mm ²)	b (mm)	b ⁺ (mm)	b ⁺⁺ (mm)	Aro (mm ²)	Aro ⁺ (mm ²)	Aro ⁺⁺ (mm ²)	b (mm)	b ⁺ (mm)	b ⁺⁺ (mm)	Aro (mm ²)	Aro ⁺ (mm ²)	Aro ⁺⁺ (mm ²)
<i>E. minima</i>	4.17 \pm 0.9	7.89	52.7	0.13 \pm 0.0	0.13	0.013	17.50 \pm 12.9	5.20	49.9	0.08 \pm 0.0	0.08	0.016	23.3 \pm 3.8	8.50	38.1	0.29 \pm 0.1	0.30	0.09
<i>L. alpina</i>	3.33 \pm 0.0	22.80	56.9	0.38 \pm 0.1	0.9	1.89	15.00 \pm 4.3	19.70	49.9	0.38 \pm 0.1	1.00	2.24	25.0 \pm 10	19.10	42.8	0.37 \pm 0.1	0.50	1.66
<i>P. alpina</i>	6.67 \pm 1.9	24.4	2.6	1.66 \pm 1.0	0.60	15.88	17.50 \pm 5.7	21.70	47.9	0.88 \pm 0.2	0.20	12.68	23.33 \pm 3.8	26.60	42.5	0.91 \pm 0.6	0.40	8.33

449

450 $df=7$ $p=0.48$; Aro:W=40 $df=7$ $p=1$;Table 4). The VRDs were different between plant species
 451 ($\chi^2:212.1$ $df:2$ $p<0.01$) and they generally differed across study sites ($\chi^2:99.7$ $df:2$ $p<0.01$). *L.*
 452 *alpina* had the widest and densest VRD followed by *P. alpina* and *E. minima* (Fig. 4; Table 4).
 453 However, the VRD for *P. alpina* tended to be deeper than for the other two plant species (Fig.
 454 4; Table 4). A clear relationship between VRD and study site was not observed, indicating that
 455 the extent and depth of the VRD was not linked to the study site (Fig. 4).

456
 457



458

459 **Figure 34.** Vertical root distribution (VRD) for (a) *Euphrasia minima*, (b) *Lecanthemopsis alpina*, and (c) *Poa alpina*.
 460 Triangles, dots and crosses represent observed values for the root cross-sectional area of all roots found at a given soil
 461 depth as described in Section 2.4. The lines portray the nls exponential models fitted to the measured data points -i.e.
 462 empirical VRD model. See online version for colours.

463

464 3.5. Influence of plant and soil attributes on key vertical root distribution parameters

465

466 The cross-validation results from fitting random forest models to the key vertical root
 467 distribution (VRD) parameters (i.e. b , Aro , and Mr ; Appendix A - Table A1 and Figure A1;
 468 Supplementary Material) suggested that the latter can be predicted successfully using the
 469 studied plant and soil attributes as predictors.

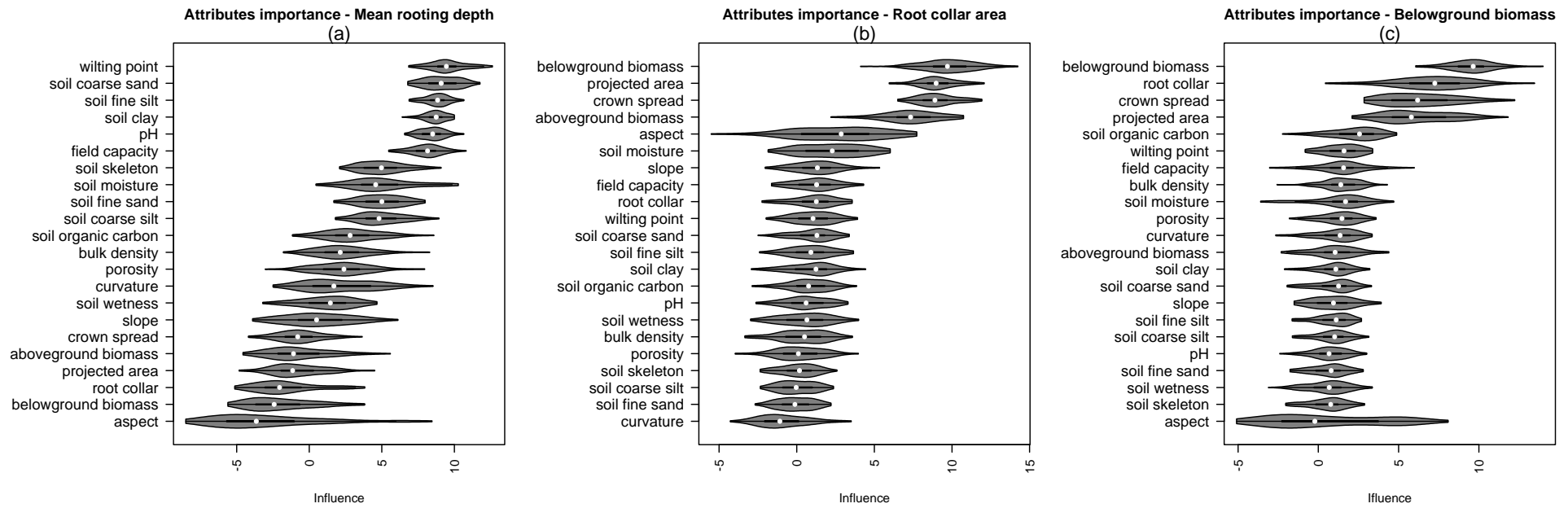


Figure 45. Violin plots depicting the influence of the studied plant and soil attributes on relevant vertical root distribution (VRD) parameters -i.e. (a) mean rooting depth, b; (b) root collar area, Aro; (c) plant belowground biomass, Mr. The white dot within the violin plot boxes represent the median while the grey area around the box represents the probability density of the data at different values.

472 The mean rooting depth (b) was chiefly influenced by soil attributes (Fig. 5a) such as the soil
473 volumetric moisture content at wilting point, followed by the soil texture (Fig. 5a). Soil pH and
474 the soil moisture at field capacity also appeared to significantly influence b (Fig. 5a). In the
475 light of the correlogram (Fig. 6), the rooting depth was strongly correlated to the soil texture,
476 positively with clay and silt contents and negatively with coarse sand content. The slope aspect,
477 the soil moisture, and organic carbon content also had a strong, positive correlation with b (Fig.
478 6). In the light of the PDPs (Appendix B - Fig. B1), there was a positive influence of the wilting
479 point on b (i.e. the higher θ_{wp} the higher b), up to 3.4 %, after which a constant effect was
480 observed. Field capacity also had a positive effect on b only detected when θ_{fc} was above 15.6
481 %. We noticed a negative influence of soil pH on b when the former was above 4.5. The
482 attributes that did not have a substantial effect on b (Fig. 5a) had a remarkable effect when the
483 PDPs were assessed (Appendix B - Fig. B1). For example, deeper root systems were found
484 under steeper conditions. However, shallower root systems were encountered when soil was
485 wetter, but shifts in the soil hydrological regime led to changes in the influence of soil moisture
486 on b . A negative effect of soil moisture on b was observed under residual and saturated regimes,
487 and a positive effect was noticed under the transitional regime. Contrariwise, soil porosity and
488 organic carbon had a positive effect on b (Tables 2 and 3; Fig. 6) which was not detected in the
489 PDPs for the soil porosity (Fig. B1).

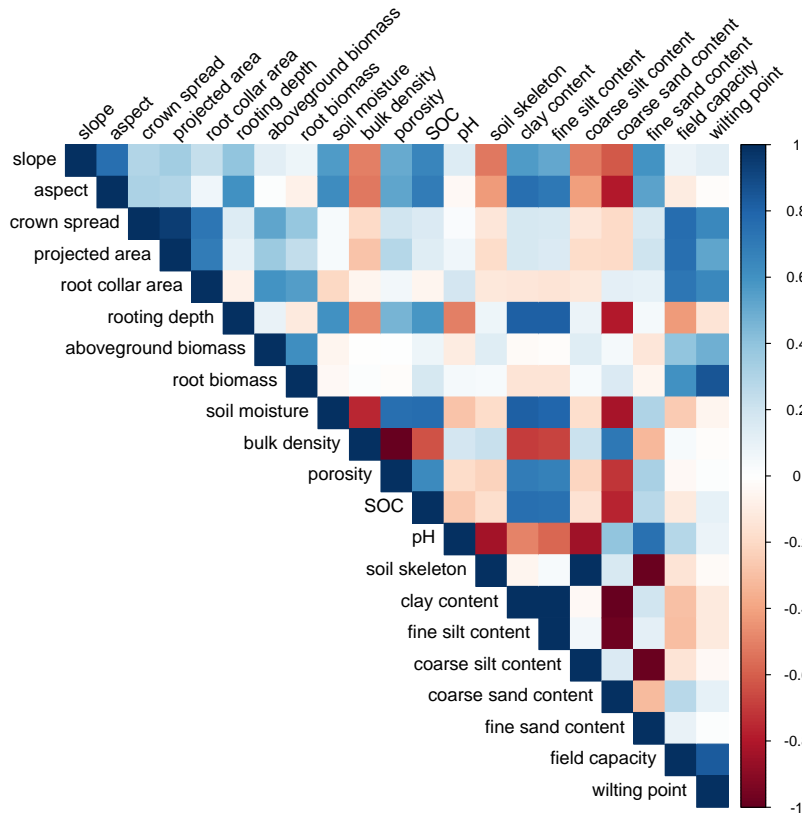
490

491 The cross-sectional area at the root collar (A_{ro}) was mostly affected by plant attributes (Fig.
492 5b). The root biomass, surface projected area, crown spread, and aboveground biomass had a
493 significant influence on A_{ro} . However, the investigated soil attributes did not have a substantial
494 influence on A_{ro} on the basis of the RF model outputs (Fig. 5b). In the light of the correlogram
495 plot (Fig. 6), A_{ro} had a strong, positive correlation with above- and belowground biomass but
496 also with the soil water content at field capacity and wilting point. According to the PDPs

497 (Appendix B - Fig. B2), all the examined plant attributes had a consistent, positive effect on
498 *Aro*. We also observed that some soil attributes had a consistent effect on *Aro* when the PDPs
499 were examined (Fig. B2) that could not be detected in the correlogram (Fig. 6) or in relative
500 influence plots (Fig. 5b). According to the PDPs, soil porosity, the percentage of clay, fine silt
501 and fine sand had a negative effect on *Aro*, while the percentage of coarse sand and coarse silt
502 had a positive effect. We also observed that *Aro* tended to be wider under steeper slope
503 conditions, and narrower when soil organic carbon increased (Fig. B2).

504

505 The root biomass (*Mr*) was predominantly influenced by plant attributes (Fig. 5c) such as the
506 aboveground biomass, *Aro*, crown spread, and plant's surface projected area. However, the
507 influence of soil organic carbon on *Mr* was significantly higher than the influence of the rest
508 of the studied soil attributes (Fig. 5c). In the light of the correlogram plot (Fig. 6), *Mr* had a
509 strong, positive correlation with the aboveground biomass, the crown spread, and *Aro*. In
510 addition, soil attributes, such as the soil moisture at field capacity and wilting point, also had a
511 strong positive correlation, with the latter being the attribute with highest correlation to *Mr*
512 (Fig. 6). According to the PDPs (Appendix B - Fig. B3), all the plant attributes studied had a
513 consistent, positive effect on *Mr*. In addition, we noticed a consistent effect of some of the soil
514 attributes studied on *Mr* which resembled the effects observed for *Aro* (Fig. B2).



515

516 *Figure 56. Correlation plot depicting Pearson's correlation coefficient between the investigated plant and soil attributes.*
 517 *Blue colour: positive correlation; Red colour: negative correlation. The darker the colour shade, the higher the correlation*
 518 *between two attributes. See online version for colours.*

519

520

521 3.6. Ecohydrological model for vertical root distribution

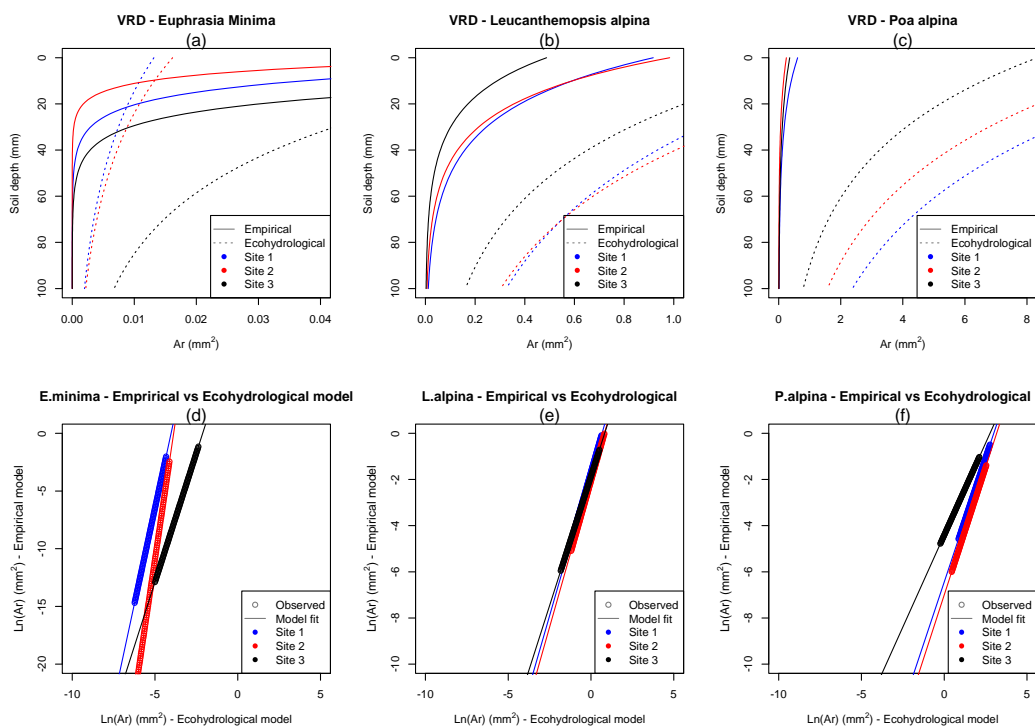
522

523 We found a substantial mismatch between the chosen parametric ecohydrological and the
 524 empirical VRD models (Figs. 8a-c; Table 4). This showed that the existing parametric,
 525 ecohydrological VRD model cannot readily predict VRD under the pedoclimatic conditions of
 526 the study area. However, we detected a consistent ($R^2 > 0.9$) linear relationship between the
 527 ecohydrological and empirical VRD models when $Ar(z)$ was log-transformed (Figs. 8d-e) -i.e.
 528 a consistent exponential fit was observed when comparing empirical, untransformed $Ar(z)$
 529 values against parametric, untransformed $Ar(z)$ values. The fitting parameters for the log-
 530 transformed linear models established between ecohydrological and empirical VRD models

531 are shown in Table 5. We observed a strong correlation ($r > 0.5$) between most of the studied
 532 plant attributes and the fitting parameters for the log-transformed linear models (Table 6). In
 533 addition, a strong correlation was observed between the fitting parameters and the soil moisture
 534 content at field capacity and at wilting point (Table 6).

535

536



537

538 *Figure 67. (a-c) Vertical root distribution (VRD) models fitted with a nls exponential model to the measured data – i.e.*
 539 *empirical VRD model (solid lines) and with the parametric, ecohydrological VRD model (dotted line) (d-e) Mathematical*
 540 *relationship between empirical and ecohydrological VRD models established with a log-transformed linear model of the*
 541 *form “ $\text{Ln}(\text{Empirical } Ar(z)) = A + B \times \text{Ln}(\text{Ecohydrological } Ar(z))$ ” (see Table 5 for fitting parameters). Also, see online version of*
 542 *this manuscript for colours.*

543
544

Table 35. Fitting parameters for the log-transformed linear model the form " $\ln(\text{Empirical } Ar(z)) = A + B \times \ln(\text{Ecohydrological } Ar(z))$ " fitted between empirical and ecohydrological VRD models.

Plant species	Site 1		Site 2		Site 3	
	A	B	A	B	A	B
<i>E. minima</i>	26.88	6.67	37.46	9.68	9.47	4.47
<i>L. alpina</i>	-1.67	2.49	-2.07	2.53	-1.86	2.24
<i>P. alpina</i>	-6.44	2.15	-7.00	2.21	-4.41	1.59

545
546
547

Table 46. Pearson's correlation coefficients for the pair-wise correlation between the evaluated soil and plant attributes and the fitting parameters for the log-transformed linear model the form " $\ln(\text{Empirical } Ar(z)) = A + B \times \ln(\text{Eco-hydrological } Ar(z))$ " fitted between empirical and ecohydrological VRD models.

Variable	A	B
Slope	-0.36	-0.42
Aspect	-0.31	-0.36
Curvature	-0.05	0.03
CS	-0.74	-0.73
Sp	-0.56	-0.58
Aro	-0.65	-0.60
Ma	-0.75	-0.68
Mr	-0.61	-0.54
b	-0.11	-0.11
θ_g	0.20	0.23
ρ_{bk}	-0.12	-0.14
n	0.18	0.20
SOC	-0.18	-0.20
pH	-0.12	-0.14
sk	-0.09	-0.16
Clay	0.19	0.29
Fine silt	-0.14	-0.16
Coarse silt	-0.12	-0.13
Fine sand	0.19	0.29
Coarse sand	-0.21	-0.31
θ_{fc}	0.16	0.19
θ_{wp}	-0.59	-0.57

548

549

550 4. Discussion

551 4.2. Vertical root distribution

552 The vertical root distribution (VRD) of the three studied alpine plant species decreased
553 exponentially with soil depth. Accordingly, VRD was successfully described with a negative
554 exponential model that was fitted to the measured data (Fig. 4). This is consistent with VRDs
555 reported for shrub, woody, and herbaceous plant species in Mediterranean (Preti et al., 2010;
556 Tron et al., 2014), southern alpine (Burylo et al., 2011) and temperate-humid ecosystems
557 (Gonzalez-Ollauri and Mickovski, 2016; Tardio et al., 2016), and it confirms that the proposed
558 approach for describing VRD in herbaceous plants is methodologically robust across terrestrial
559 ecosystems in Europe.

560

561 We attributed the observed VRD differences across plants and sites (Fig. 4) to the differences
562 in plant attributes that we found (Table 3). In spite of the differences observed in key VRD
563 parameters across sites (Table 3), and of the strong influence of site-specific attributes on the
564 key VRD parameters that we noticed herein (Fig. 5 and Section 4.2), the direction of the effect
565 of the study site on the size and depth of the measured VRDs was unclear, given that the extent
566 of VRD changed with the plant species from site to site (Fig. 4). Yet, there were limitations to
567 the study, as we did not evaluate altitudinal differences between plant individuals (e.g. Gale,
568 2004; Miyamoto et al., 2015), nor the differences in soil nutrients between sampling locations
569 (e.g. Forde and Lorenzo, 2001), or the climatic differences across study sites (Schenk and
570 Jackson, 2005). We think that all these aspects deserve further consideration to expand on our
571 findings related to how VRD is shaped by local site conditions.

572

573 The proposed VRD description approach has been used effectively in woody plant species
574 under both sloped and flat topographies (Tron et al., 2014; Tardio et al., 2016; Gonzalez-Ollauri
575 et al., 2020). Still, its ability to capture realistically large roots (> 3 mm in diameter, incl. tap
576 roots) in woody plants needs further verification, notwithstanding the fact that the *in situ*
577 description of root systems for woody plants is methodologically challenging (Böhm, 1979),
578 and it generally focuses on one or two vertical profiles of the root system (e.g. Tardio et al.,
579 2016; Gonzalez-Ollauri et al., 2020) from which it is hard to comprehensively capture root
580 system features. However, the VRD description approach followed herein is methodologically
581 simple and easy to implement, it provided a good and realistic picture of the VRD for the
582 studied alpine plants with root systems mainly comprising fine roots, and it generated
583 information directly applicable in workflows needing VRD information such as plant-water
584 uptake models (e.g. Laio, 2006; Shukla, 2014) or soil-root reinforcement estimation
585 approaches (e.g. Gonzalez-Ollauri and Mickovski, 2016, 2017b; Kokutse et al., 2016).

586

587 4.3. Influence of climate, plant and soil attributes on key vertical root distribution parameters

588

589 The rooting depth (b) and root biomass (Mr) for the three studied plant species (Table 3) were
590 within the ranges described in Pohl et al. (2011) and Hudek et al. (2017) for alpine ecosystems.
591 However, these were below the ranges reported for semi-arid (Preti et al., 2010) and temperate-
592 humid (Gonzalez-Ollauri and Mickovski, 2016) climates. These differences were attributed to
593 the short duration of the growing season in our study area, and associated to long periods with
594 snow cover and low temperatures, which likely limited plant development (e.g. Kaspar and
595 Bland, 1992; Lahti et al., 2005; Alvarez-Uria and Körner, 2007).

596

597 The key studied VRD parameters (i.e. b : mean rooting depth; A_{ro} : cross-sectional area at the
598 root collar; and M_r : root biomass) were distinctly influenced by the investigated soil and plant
599 attributes (Figs 6, 7 and Appendix B – Figs. B1-B3). We observed that, while the rooting depth
600 was mostly site-specific, the allocation of biomass to the belowground plant parts and its
601 distribution along the soil profile was both species-specific and reliant on relevant soil
602 ecohydrological features.

603

604 4.3.1. Rooting depth

605

606 The mean rooting depth (b ; Laio et al., 2006) was chiefly influenced by soil attributes
607 governing the water available to plants in the soil (WAP; i.e. difference between soil water
608 content at field capacity (θ_{fc}) and wilting point (θ_{wp}); Fig. 5a, 7 and Appendix B – Fig. B1;
609 Table 4; Eq.4 Table 1; Casper et al., 2003). It is worth noting that θ_{fc} and θ_{wp} were estimated
610 in the light of well-established pedotransfer functions nested in the VRD model (Eqs. 4, 5, 11
611 and 12; Table 1) with relatively low sensitivity (Gonzalez-Ollauri and Mickovski, 2016) and
612 which employed soil texture, soil organic carbon, and porosity as inputs (Toth et al., 2015).
613 Accordingly, soils with high organic carbon and with a fine texture (i.e. high clay and silt
614 content) would have high water retention capacity (Kirkham, 2005; Lu and Likos, 2004) and,
615 as a result, deeper root systems, as it was shown herein (Figs. 6 and B1; Table 3; Schenk and
616 Jackson, 2005; Gonzalez-Ollauri and Mickovski, 2016). In fact, we observed clear differences
617 across sites in terms of the soil attributes governing WAP (Table 2), which may explain why
618 Site 3 had substantially deeper rooting depths than sites 1 and 2 (Table 3). The effect of the
619 soil's ecohydrological characteristics on the rooting depth has been highlighted in previous
620 studies (e.g. Schenk, 2005; Laio et al., 2006; Preti et al., 2010), suggesting that the ability of
621 roots to explore the soil in depth largely depends on the water mass balance within the topsoil

622 (Tsutsumi et al., 2003; Laio, 2006; Laio et al., 2006). In fact, the soil water mass balance
623 features in the proposed ecohydrological models predicting the mean rooting depth (Eqs. 4 and
624 5; Table 1; Laio et al., 2006; Gonzalez-Ollauri and Mickovski, 2016), and our results validate
625 that these models are conceptually correct. However, other models are nested into the
626 investigated VRD model (e.g. growing season duration, evapotranspiration, soil pedotransfer
627 functions, etc.), leading to likely propagation of errors and uncertainty (Taylor, 1997) that
628 should be thoroughly investigated and dealt with prior to verifying the quality and robustness
629 of the VRD models (e.g. Gonzalez-Ollauri and Mickovski, 2017b).

630

631 Model differences between the options for arid or semi-arid (Eq. 4; Table 1) and temperate
632 humid (Eq.5; Table 1) climates imply rooting depth differences that were not tested herein. In
633 arid climates, water withdrawal through evapotranspiration limits the amount of water
634 available to plants in the topsoil, thus encouraging deeper rooting depths than in humid
635 climates. By contrast, in temperate humid climates, water inputs exceed outputs in the topsoil
636 (i.e. rainfall > evapotranspiration), leading to shallower rooting depths as roots do not face
637 water limitations in the topsoil - i.e. roots do not need to explore the soil in search of deep water
638 (Schenk and Jackson, 2005). In alpine climates, however, where snowfall, ground frost, and
639 short snow-free periods govern the soil ecohydrological behaviour (e.g. Molotch et al., 2009),
640 further model tuning is needed to fully capture the rooting depth and VRD with the proposed
641 parametric ecohydrological model (Fig. 7a-c; Table 4). In addition, the direct quantification of
642 soil attributes governing the available water to plants through, for example, retrieving the soil-
643 water retention function (e.g. Zhang et al., 2019) or by evaluating the soil structure and
644 aggregates (e.g. Bengough, 2003) could shed more light on the effect of the soil's
645 ecohydrological characteristics on the rooting depth and VRD.

646

647 It is also worth noting the high influence of soil pH on the rooting depth (Fig. 4a; Fig. 6), which
648 on the basis of the correlogram (Fig. 6) and PDPs (Annex B – Fig.B1) was negative – i.e.
649 shallower rooting depths were noticed when the pH was higher. This observation may indicate
650 that plants tend to reduce root elongation and increase thickness as a strategy to promote
651 nutrient uptake when soil pH is high (e.g. Robles-Aguilar et al., 2019). The latter is somehow
652 supported by the positive interaction that we observed between soil pH and the cross-sectional
653 area at the root collar (*A_{ro}*; Figs. 6 and B2), suggesting that root thickness increased at the
654 collar when soil pH increased. Yet, as the variability in soil pH was small across study sites
655 (Table 3), we cannot convincingly elucidate possible reasons behind our observations and we
656 thus recommend further research on the effect of soil pH on the key VRD parameters.

657

658 In this study, there were also limitations to the analysis because site-specific records for the
659 climate attributes and for the snowpack depth, although capable of affecting the rooting depth
660 in alpine ecosystems (e.g. Cooper et al., 2011), were not available. Additionally, we did not
661 consider the topographical effect of the slope gradient on the rainfall lost to runoff and, in turn,
662 on the rooting depth (Tron et al., 2014; Tardio et al., 2016); nor the influence of preferential
663 flow paths in the soil (e.g. Clothier et al., 2008; Gonzalez-Ollauri et al., 2020) or the effect of
664 soil anisotropy on the rooting depth and VRD. We believe that all these aspects deserve detailed
665 consideration to improve the predictive capacity of the parametric VRD models studied here.
666 However, the consistent linear relationship between empirical and parametric ecohydrological
667 VRD models reported in this study (Fig. 7d-e), and the high correlation found between fitting
668 parameters and soil attributes governing the available water to plants (i.e. θ_{fc} and θ_{wp} ; Table
669 6) set the direction of future research.

670

671 4.3.2. Cross-sectional area at the root collar and root biomass

672

673 The cross-sectional area at the root collar (A_{ro}) and the root biomass (M_r) were mostly
674 influenced by the investigated plant attributes (Fig. 5 and Appendix B – Figs. B2 and B3).
675 However, a substantial effect of the soil water at field capacity and wilting point on A_{ro} and
676 M_r was also detected (Fig. 6). It is worth noting that the combined effect of the soil and plant
677 attributes on the key VRD parameters was only evident when multiple data analysis approaches
678 were used together - i.e. relative influence from RF models (Fig. 5), pairwise correlation (Fig.
679 6) and PDPs (Appendix B), indicating that comprehensive data mining is needed to fully grasp
680 complex interactions between environmental variables affecting VRD (Supplementary
681 Material - Fig. S1). The findings shown herein corroborate that while the extent of the root
682 system in the soil (i.e. rooting depth; Section 4.2.1) is delimited by the soil water mass balance
683 and its contributing soil attributes (i.e. soil texture, SOC , θ_{fc} and θ_{wp} ; Figs. 5a and 6), the plant
684 biomass allocated belowground is distributed along the VRD profile in the light of both plant-
685 specific and soil attributes (Figs. 6b-c and 7). The latter aspect features in the proposed VRD
686 model through A_{ro} (Eq.3; Table 1), which acts as scaling factor in the distribution of root
687 biomass along the root profile in the soil (Preti et al., 2010; Gonzalez-Ollauri and Mickovski,
688 2016). In this regard, we noticed that the magnitude of A_{ro} was positively influenced by the
689 slope gradient whilst being negatively affected by SOC (Fig. B2). A plausible explanation for
690 the former is that plants tend to adopt anchoring strategies in steep slopes (e.g. Tardio et al.,
691 2016), which may imply the allocation of root biomass near the ground surface to promote
692 anchorage to the ground and plant stability (Chiatante et al., 2003). In fact, we also noticed that
693 M_r was higher on steeper slopes (Fig. B3). Contrariwise, root biomass tends to be distributed
694 towards deeper portions of the soil when there is more SOC , which would reduce the amount
695 of root biomass allocated near the surface (Fig. B3) and thus to A_{ro} . All these aspects support
696 the assumption of using a ‘cone-shape-volume’ to model the distribution of root biomass in the

697 soil (Fig. 3b; Supplementary Material), which was further supported by the strong influence of
698 Mr on Aro (Figs. 6b and 7). However, the observed mismatch between empirical and parametric
699 ecohydrological VRD models (Fig. 7a-c; Table 4), in which Aro , Mr , and b are embedded
700 (Table 1), suggests that the modelling approach to estimate the key VRD parameters Aro and
701 b (Eqs. 4, 5 and 7; Table 1) must be revised for alpine ecosystems. Future work may consider
702 to explore the effect of topography in detail and/or to include climate-specific variables such
703 as snowpack depth, duration of the snow-free period, and frozen ground cycle, and how these
704 influence AWP and Aro in alpine ecosystems. In addition, soil nutrient limitations (e.g.
705 nitrogen; Zong et al., 2020) and plant-specific aspects related to growth and survival strategies
706 of alpine plants (e.g. Cooper et al., 2003; Germino, 2014) can be considered in future versions
707 of the VRD model to portray more realistically the characteristic allocation of plant biomass
708 above- and belowground in alpine ecosystems (e.g. Wu et al., 2013).

709

710 Nonetheless, the strong correlation between the investigated plant attributes and the fitting
711 parameters resulting from evaluating the relationship between empirical and parametric,
712 ecohydrological VRD models (Table 6) suggests that the collection of studied plant attributes
713 was appropriate, setting the direction of future research. The strong influence of plant attributes
714 such as the crown spread and projected area on the plant aboveground biomass (Ma) and Aro
715 (Figs. 6b-c, 7, Appendix B – Figs. B2 and B3) hints at the possibility of establishing robust
716 data-mining approaches able to predict VRD on the basis of easy-to-measure aboveground
717 plant attributes (e.g. Fig. 3); provided that information on the allometry relationship between
718 above and belowground plant parts is available (Table 2; e.g. Cheng and Niklas, 2007). In this
719 regard, we expected that the allometry ratio (i.e. $ALR=Mr/Ma$; Table 2) would be consistently
720 above unity in the studied alpine plant species (e.g. Pohl et al., 2011), as a greater allocation of
721 biomass to the belowground plant parts could help plants to withstand harsh aboveground

722 conditions (Germino, 2014). Nonetheless, only *P. alpina* had an *ALR* consistently above unity.
723 Future work helping to establish consistent and site-specific allometry relationships between
724 above and belowground plant parts in alpine ecosystems (e.g. Štastná et al. 2012) will
725 undoubtedly help to consolidate approaches seeking to describe VRD using very few, easily
726 measurable, parameters, like the one discussed herein.

727

728 5. Conclusion

729 Our study consolidates a simple protocol to describe the vertical root distribution (VRD) in
730 herbaceous plants. It also addresses, for the first time, the influence of soil and plant attributes
731 on key VRD parameters, validating the principles and assumptions behind the existing
732 parametric, ecohydrological models predicting VRD, and casting light on how VRD can be
733 effectively described using simple climate, soil and plant attributes. In fact, we confirmed that
734 insights into the water mass balance in the soil and into the water available to plants are crucial
735 to describe VRD in alpine ecosystems, as it has been suggested in previous studies for semi-
736 arid and temperate humid ecosystems. However, the existing parametric ecohydrological VRD
737 models were not able to portray successfully the vertical root distribution of the studied alpine
738 plants in the light of the measured root profiles. Although we found a strong correlation
739 between empirical and parametric VRD models that establish a clear direction for future
740 research, we also think that the parametric VRD model needs to be revised in the future to
741 include features affecting the water available to plants in alpine ecosystems, such as the
742 snowpack characteristics or the length of the snow-free and frozen ground periods. We also
743 encourage future work exploring in detail the effect of topography, elevation, climate and
744 nutrient limitations on VRD, as these factors can help to formulate new models predicting VRD
745 realistically.

746

747 CRediT authorship contribution statement

748 Alejandro Gonzalez-Ollauri: funding acquisition, conceptualization, methodology, data

749 curation, formal analysis, investigation, project administration, writing - original draft, writing

750 – review & editing

751 Csilla Hudek: investigation, writing – review & editing

752 Slododan B. Mickovski: funding acquisition, methodology, project administration, writing –

753 review & editing

754 Davide Viglietti: investigation

755 Nicole Ceretto: investigation

756 Michele Freppaz: project administration, resources, writing – review & editing

757

758 Acknowledgement

759

760 We acknowledge the useful comments and suggestions from three anonymous referees and the

761 Editor that helped us to improve the manuscript. The contribution of A. Gonzalez-Ollauri and

762 S.B. Mickovski was funded by Erasmus+ project ECOMED (575796-EPP-1-2016-ES-

763 EPPKA2-KA) and the Green4Brown Project (M315-10363) funded by the BEAM Research

764 Centre of the Glasgow Caledonian University.

765

766

767 6. References

768

769 Alvarez-Uria, P., Körner, C., 2007. Low temperature limits of root growth in deciduous and

770 evergreen temperate tree species. *Funct. Ecol.* 21, 211–218.

771 Arnone, E., Caracciolo, D., Noto, L. V., Preti, F., and Bras, R. L., 2016. Modeling the
772 hydrological and mechanical effect of roots on shallow landslides, *Water Resour.*
773 *Res.*, 52, 8590– 8612, doi:[10.1002/2015WR018227](https://doi.org/10.1002/2015WR018227).

774 ASTM (1995) D 4972-95a: Standard test method for pH of soils. ASTM International, West
775 Conshohocken, PA, USA.

776 Asturnauta, 2020. *Euphrasia minima*. [https://www.asturnatura.com/especie/euphrasia-](https://www.asturnatura.com/especie/euphrasia-minima.html)
777 [minima.html](https://www.asturnatura.com/especie/euphrasia-minima.html). Retrieved on 07/07/2020.

778 Bengough A.G. (2003) Root Growth and Function in Relation to Soil Structure,
779 Composition, and Strength. In: de Kroon H., Visser E.J.W. (eds) Root Ecology.
780 Ecological Studies (Analysis and Synthesis), vol 168. Springer, Berlin, Heidelberg.
781 https://doi.org/10.1007/978-3-662-09784-7_6

782 Blozan, W., 2008. Tree measuring guidelines of the eastern native tree society. Bull. East.
783 Native Tree Soc. 1 (1), 3–10.

784 Böhm, W., 1979. Methods of Studying Root Systems. Springer Verlag, Berlin.

785 Breiman, L., 2001. Random forests. Mach. Learn. 45, 5–32.

786 Burylo, M., Hudek, C., Rey, F., 2011. Soil reinforcement by the roots of six dominant species
787 on eroded mountainous marly slopes (Southern Alps, France). *Catena*, 84: 70-78.

788 Burylo, M., Dutoit, T. and Rey, F., 2014. Species Traits as Practical Tools for Ecological
789 Restoration of Marly Eroded Lands. *Restor Ecol*, 22: 633-640. doi:[10.1111/rec.12113](https://doi.org/10.1111/rec.12113)

790 Casper, B.B., Schenk, H.J., Jackson, R.B., 2003. Defining a Plant's Belowground Zone of
791 Influence. *Ecology* 84 (9), 2313–2321.

792 Cheng, D., Niklas, K.J., 2007. Above- and below-ground biomass relationships across 1534
793 forested communities. *Ann. Bot.* 99, 95–102.

794 Chiatante, D., Scippa, S.G., Di Lorio, A., Sarnataro, M., 2003. The influence of steep slopes
795 on root system development. *J. Plant Growth Regul.* 21, 247–260.

796 Clothier, B.E., Green, S.R. and Deurer, M., 2008. Preferential flow and transport in soil:
797 progress and prognosis. *European Journal of Soil Science*, 59: 2-13. doi:[10.1111/j.1365-
798 2389.2007.00991.x](https://doi.org/10.1111/j.1365-2389.2007.00991.x)

799 Cooper, E., Dullinger, S., Semenchuk, P., 2011. Late snowmelt delays plant development and
800 results in lower reproductive success in the High Arctic. *Plant science*, 180:157-67.
801 [10.1016/j.plantsci.2010.09.005](https://doi.org/10.1016/j.plantsci.2010.09.005).

802 Coutts, M.P., Nielsen, C.C.N., Nicoll, B.C., 1999. The development of symmetry, rigidity and
803 anchorage in the structural root system of conifers. *Plant and Soil* 217, 1-15.

804 Darwin, C., 1880. *The Power of Movement in Plants*. John Murray, London, UK.

805 Fitter, A.H., Stickland, T.R., 1991. Architectural analysis of plant root systems 2. Influence of
806 nutrient supply on architecture in contrasting plant species. *New phytologist*, 118: 383-
807 389.

808 Forde, B., Lorenzo, H., 2001. The nutritional control of root development. *Plant and*
809 *Soil*, **232**: 51–68. <https://doi.org/10.1023/A:1010329902165>

810 Freppaz, M., Filippa, G., Caimi, A., et al., 2010. Soil and plant characteristics in the alpine
811 tundra (NW Italy). In: *Tundras: Vegetation, Wildlife and Climate Trends*. Nova Publishers.
812 pp 81–110.

813 Freppaz, M., Viglietti, D., Balestrini, R., Lonati, M., Colombo, N., 2019. Climatic and
814 pedoclimatic factors driving C and N dynamics in soil and surface water in the alpine tundra
815 (NW-Italian Alps). *Nature Conservation*, 34: 67-90.

816 Fuller, W. A. 1987. *Measurement Error Models*. John Wiley & Sons. ISBN 978-0-471-86187-
817 4.

818 Gale J. (2004). Plants and altitude--revisited. *Annals of botany*, 94(2), 199.
819 <https://doi.org/10.1093/aob/mch143>

820 Germino M.J. 2014. *Plants in Alpine Environments*. In: Monson R. (eds) *Ecology and the*
821 *Environment*. Springer, New York, NY

822 Goodman, A.M., Ennos, A.R., 1999. The Effects of Soil Bulk Density on the Morphology and
823 Anchorage Mechanics of the Root Systems of Sunflower and Maize. *Annals of Botany*, 83:
824 293-302.

825 Gonzalez-Ollauri, A., Mickovski, S.B., 2016. Using the root spread information of pioneer
826 plants to quantify their mitigation potential against shallow landslides and erosion. *Ecol. Eng.*
827 95, 302–315.

828 Gonzalez-Ollauri, A., Mickovski, S.B., 2017a. Plant-soil reinforcement response under
829 different soil hydrological regimes. *Geoderma* 285, 141–150.

830 Gonzalez-Ollauri, A. and Mickovski, S.B., 2017b. Plant-Best: A novel plant selection tool for
831 slope protection. *Ecological Engineering* 106 (2017) 154–173

832 Gonzalez-Ollauri, A. and Mickovski, S.B., 2017c. Shallow landslides as drivers for slope
833 ecosystems evolution and biophysical diversity. *Landslides*, 14(5), 1699-1714. DOI
834 10.1007/s10346-017-0822-y

835 Gonzalez-Ollauri, A., Mickovski, S.B., 2018. Green for Brown (G4B): A Novel Tool for
836 Evaluating Phytoextraction in Soils Polluted by Heavy Metals. In: Kallel A., Ksibi M., Ben

837 Dhia H., Khélifi N. (eds) Recent Advances in Environmental Science from the Euro-
838 Mediterranean and Surrounding Regions. EMCEI 2017. Advances in Science, Technology &
839 Innovation (IEREK Interdisciplinary Series for Sustainable Development). Springer, Cham.
840 http://doi-org-443.webvpn.fjmu.edu.cn/10.1007/978-3-319-70548-4_81

841 Gonzalez-Ollauri, A., Stokes, A., Mickovski, S.B., 2020. A novel framework to study the effect
842 of tree architecture in stemflow yield and its consequences for soil-water dynamics. *Journal of*
843 *Hydrology*, 582: 124448.

844 Greenwell, B.M., 2017. pdp: An R package for constructing partial dependence plots. *R J.* 9
845 (1), 421–436.

846 Greve, P., Roderick, M.L., Ukkola, A.M., Wada, Y., 2019. The aridity index under global
847 warming. *Environ. Res. Lett.*, 14: 124006.

848 Hastie, T., Tibshirani, R., Friedman, J., 2009. *The Elements of Statistical Learning*, Second
849 Edition, Section 10.13.2, Springer, 2009.

850 Head, K.H., 1980. *Manual of Soil Laboratory Testing*. CRC Press, Boca Raton,US.

851 Herbert, D.A., Rastetter, E.B., Gough, L., Shaver, G.R., 2004. Species diversity across
852 nutrient gradients: an analysis of resource competition in model ecosystems. *Ecosystems*
853 7:296–310

854 Hudek, C., Stanchi, S., D'Amico, M., Freppaz, M., 2017a. Quantifying the contribution of the
855 root system of alpine vegetation in the soil aggregate stability of moraine. *International Soil*
856 *and Water Conservation Research*, 5: 36-42.

857 Hudek, C., Sturrock, C.J., Atkinson, B.S., Stanchi, S., Freppaz, M., 2017b. Root morphology
858 and biomechanical characteristics of high-altitude alpine plant species and their potential in
859 soil stabilization. *Ecological Engineering*, 109, Part B: 228-239.

860 Iversen, C. M., Sloan, V.L., Sullivan, P.F., Euskirchen, E.S., McGuire, A.D., Norby, R.J.,
861 Walker, A.P., Warren, J.M., Wullschleger, S.D., 2014. The unseen iceberg: plant roots in arctic
862 tundra. *New Phytologist*, 205: 34-58.

863 Jackson, R.B., Canadell, J., Ehleringer, J.R., Mooney, H.A., Sala, O.E., Schulze, E.D., 1996.
864 A global analysis of root distributions for terrestrial biomes. *Oecologia* 108, 389–411.

865 Jarvis, N., 1989. A simple empirical model of root water uptake. *Journal of Hydrology*,
866 107:57-72.

867 Kaspar, T.C., Bland, W. L., 1992. Soil temperature and root growth. *Soil Science*,
868 154(4):290-299.

869 Kirkham, M. B., 2005. *Principles of Soil and Water Retentions*. Elsevier, Amsterdam, NL.

870 Kleidon, A., 2004. Global datasets of rooting zone depth inferred from inverse methods, *J.*
871 *Clim.*, 17(13), 2714– 2722.

872 Kokutse, N. K., Tranquille Temgoua, A. G., Kavazović,Z., 2016. Slope stability and
873 vegetation: Conceptual and numerical investigation of mechanical effects. *Ecological*
874 *Engineering*, 86:146-153, <https://doi.org/10.1016/j.ecoleng.2015.11.005>.

875 Köppen, W., 1884. The thermal zones of the Earth according to the duration of hot, moderate
876 and cold periods and the impact of heat on the organic world. *Meteorol. Z.* 1, 215–226.

877 Köstler, J. N., Brückner, E., et Bibelriether, H. 1968: *Die Wurzeln der Waldbau* 1me edn.
878 Verlag Paul Parey.

879 Kuhn, M. et al., 2018. caret: Classification and Regression Training. R package version 6.
880 0.81. <https://CRAN.R-project.org/package=caret>.

881 Kutschera L., Lichtenegger E., 1992. Wurzelatlas mitteleuropäischer Grünlandpflanzen. Band
882 2: Pteridophyta und Dicotyledoneae; Teil 1: Morphologie, Anatomie, Ökologie, Verbreitung,
883 Soziologie, Wirtschaft. Gustav Fischer, Stuttgart

884 Laio, F., 2006. A vertically extended stochastic model of soil moisture in the root zone. *Water*
885 *Resources Research*, 42:W02406

886 Laio, F., D'Odorico, P., Ridolfi, L., 2006. An analytical model to relate the vertical root
887 distribution to climate and soil properties. *Geophys. Res. Lett.*, 33 (2006), p. L18401

888 Lahti, M., Aphalo, P., Finér, L., Ryyppö, A., Lehto, T., Mannerkoski, H., 2005. Effects of soil
889 temperature on shoot and root growth and nutrient uptake of 5-year-old Norway spruce
890 seedlings. *Tree physiology*, 25: 115-22. 10.1093/treephys/25.1.115.

891 Liaw, A., Wiener, M., 2002. Classification and Regression by randomForest. *R News* 2(3):
892 18-22.

893 Lu, N., Likos, W.J., 2004. *Unsaturated Soil Mechanics*. John Wiley and Sons, Hoboken,
894 US.

895 Lucherini, A., Gonzalez-Ollauri, A., Mickovski, S.B., 2020. The effect of vegetation on soil
896 polluted with galligu: phytostabilisation and novel approaches to evaluate soil galligu
897 concentration. *Environmental Geotechnics*, <https://doi.org/10.1680/jenge.19.00031>

898 Lynch, J., 1995. Root architecture and plant productivity. *Plant Physiol.* 109:7-13.

899 Matthies, D. 1998. Influence of the host on growth and biomass allocation in the two facultative
900 root hemiparasites *Odontites vulgaris* and *Euphrasia minima*. *Flora* (1998) 193, 187-193

901 McMaster, G.S., Wilhelm, W.W., 1997. Growing degree-days: one equation, two
902 interpretations. *Agric. Forest Meteorol.* 87, 291–300.

903 Mickovski, S.B., van Beek, L.P.H. & Salin, F. Uprooting of Vetiver Uprooting Resistance of
904 Vetiver Grass (*Vetiveria zizanioides*). *Plant Soil* 278, 33–41 (2005).

905 Miyamoto, K., Wagai, R., Aiba, S. *et al.* Variation in the aboveground stand structure and
906 fine-root biomass of Bornean heath (kerangas) forests in relation to altitude and soil nitrogen
907 availability. *Trees* 30, 385–394 (2016). <https://doi.org/10.1007/s00468-015-1210-7>

908 Molotch, N.P., Brooks, P.D., Burns, S.P., Litvak, M., Monson, R.K., McConnell, J.R. and
909 Musselman, K. (2009), Ecohydrological controls on snowmelt partitioning in mixed-conifer
910 sub-alpine forests. *Ecohydrol.*, 2: 129-142. doi:[10.1002/eco.48](https://doi.org/10.1002/eco.48)

911 Pierce, S., Stirling, C. M., Baxter, R., 2000. Architectural and physiological heterogeneity
912 within the synflorescence of the pseudoviviparous grass *Poa alpina* var. *vivipara* L. *Journal of*
913 *Experimental Botany*, 51(351):1705-1712.

914 Pohl, M., Stroude, R., Buttler, A., Rixen, C., 2011. Functional traits and root morphology of
915 alpine plants. *Annals of Botany*, 108: 537-545.

916 Preti, F., Giadrossich, F., 2009. Root reinforcement and slope bioengineering sta- bilization
917 by Spanish Broom (*Spartium junceum* L.). *Hydrol. Earth Syst. Sci.* 13, 1713–1726.

918 Preti, F., Dani, A., Laio, F., 2010. Root profile assessment by means of hydrological,
919 pedological and above-ground vegetation information for bio-engineering purposes.
920 *Ecological Engineering*, 36:305-316.

921 Preti, F., 2013. Forest protection and protection forest: Tree root degradation over hydrological
922 shallow landslides triggering. *Ecological Engineering*, 61P:633-645.

923 Priestley, C., Taylor, R., 1972. On the assessment of surface heat flux and evaporation using
924 large-scale parameters. *Mon. Weather Rev.* 100 (2), 81–92.

925 Quine, C.P., Burnand, A.C., Coutts, M.P., Reynard, B.R., 1991. Effects of mounds and

926 stumps on the root architecture of Sitka spruce on a peaty gley restocking site. *Forestry* 64,
927 385-401.

928 R Core Team, 2018. R: A Language and Environment for Statistical Computing. R
929 Foundation for Statistical Computing, Vienna, Austria <https://www.R-project.org/>.

930 Rodríguez-Iturbe, I., & Porporato, A., 2005. *Ecohydrology of Water-Controlled Ecosystems:*
931 *Soil Moisture and Plant Dynamics*. Cambridge: Cambridge University Press.
932 doi:10.1017/CBO9780511535727

933 Schenk, H.J., Jackson, R.B., 2005. Mapping the global distribution of deep roots in relation to
934 climate and soil characteristics. *Geoderma* 126, 129–140.

935 Schenk, H., 2005. Vertical vegetation structure below ground: scaling from root to globe.
936 *Progr. Bot.* 66, 341–373.

937 Shukla M. (2014) *Soil Physics: An Introduction*. Boca Raton, Florida: CRC Press.

938 Šťastná, P., Klimešová, J., Doležal, J., 2012. Altitudinal changes in the growth and allometry
939 of *Rumex alpinus*. *Alp Botany* 122, 35–44. <https://doi.org/10.1007/s00035-012-0099-7>
940

941 Stokes, A., Atger, C., Bengough, A.G., Fourcaud, T., Sidle, R.C., 2009. Desirable plant root
942 traits for protecting natural and engineered slopes against landslides. *Plant and Soil* 324 (1), 1–
943 30.

944 Strobl, C., Boulesteix, A., Kneib, T. *et al.*, 2008. Conditional variable importance for random
945 forests. *BMC Bioinformatics* 9, 307. <https://doi.org/10.1186/1471-2105-9-307>

946 Tardio, G., Gonzalez-Ollauri, A., Mickovski, S.B., 2016. A non-invasive root distribution
947 analysis methodology from a slope stability approach. *Ecol. Eng.* 97, 46–57.

948 Taub, D.R., Goldberg, D., 1996. Root system topology of plants form habitats differing in soil
949 resource availability. *Functional Ecology* 10, 258-264.

950 Taylor, J. R., 1997. An introduction to error analysis: The study of uncertainties physical
951 measurements (2nd Edition). University Science Books, CA, USA.

952 Toth, B., Weynants, M., Nemes, A., Mako, A., Bilas, G., Toth, G., 2015. New generation of
953 hydraulic pedotransfer functions for Europe. *Eur. J. Soil Sci.* 66, 226–238.

954 Tron, S., Dani, A., Laio, F., Preti, F., Ridolfi, L., 2014. Mean root depth estimation at
955 landslide slopes. *Ecol. Engine* 69, 118–125.

956 Tsutsumi, D., Kosugi, K., Mizuyama, T., 2003. Effect of hydrotropism on root system
957 development in soybean (*Glycine max*): growth experiments and model simulation. *J. Plant*
958 *Growth Regul.* 21, 441–458.

959 Ukwildflowers (2020). *Lucanthemopsis alpina*.
960 [https://www.ukwildflowers.com/Web_pages/leucanthemopsis_alpina_alpine_moon_daisy.ht](https://www.ukwildflowers.com/Web_pages/leucanthemopsis_alpina_alpine_moon_daisy.htm)
961 [m](https://www.ukwildflowers.com/Web_pages/leucanthemopsis_alpina_alpine_moon_daisy.htm)). Retrieved on 07/07/2020.

962 van Wijk, M. T., and Bouten, W., 2001). Towards understanding tree root profiles: Simulating
963 hydrologically optimal strategies for root distribution, *Hydrol. Earth Syst. Sci.*, 5(4), 629– 644.

964 Verma, P, George, KV, Singh, HV, Singh, SK, Juwarkar, A, Singh, RN, 2006. Modeling
965 rhizofiltration: heavy-metal uptake by plant roots. *Environmental Modeling and Assessment*,
966 11, 387-394.

967 Waisel, Y., Eshel, A., Kafkafi. U., (Eds.) 2002. *Plant Roots: The Hidden Half*, Marcel Dekker,
968 New York.

969 Wu, J., Shen, Z., Zhang, X. et al. Biomass allocation patterns of alpine grassland species and
970 functional groups along a precipitation gradient on the Northern Tibetan Plateau. *J. Mt. Sci.*
971 10, 1097–1108 (2013). <https://doi.org/10.1007/s11629-013-2435-9>

972 Zeng, X. 2001. Global Vegetation Root Distribution for Land Modeling. *Journal of*
973 *Hydrometeorology*, 2 (2001): 525-530.

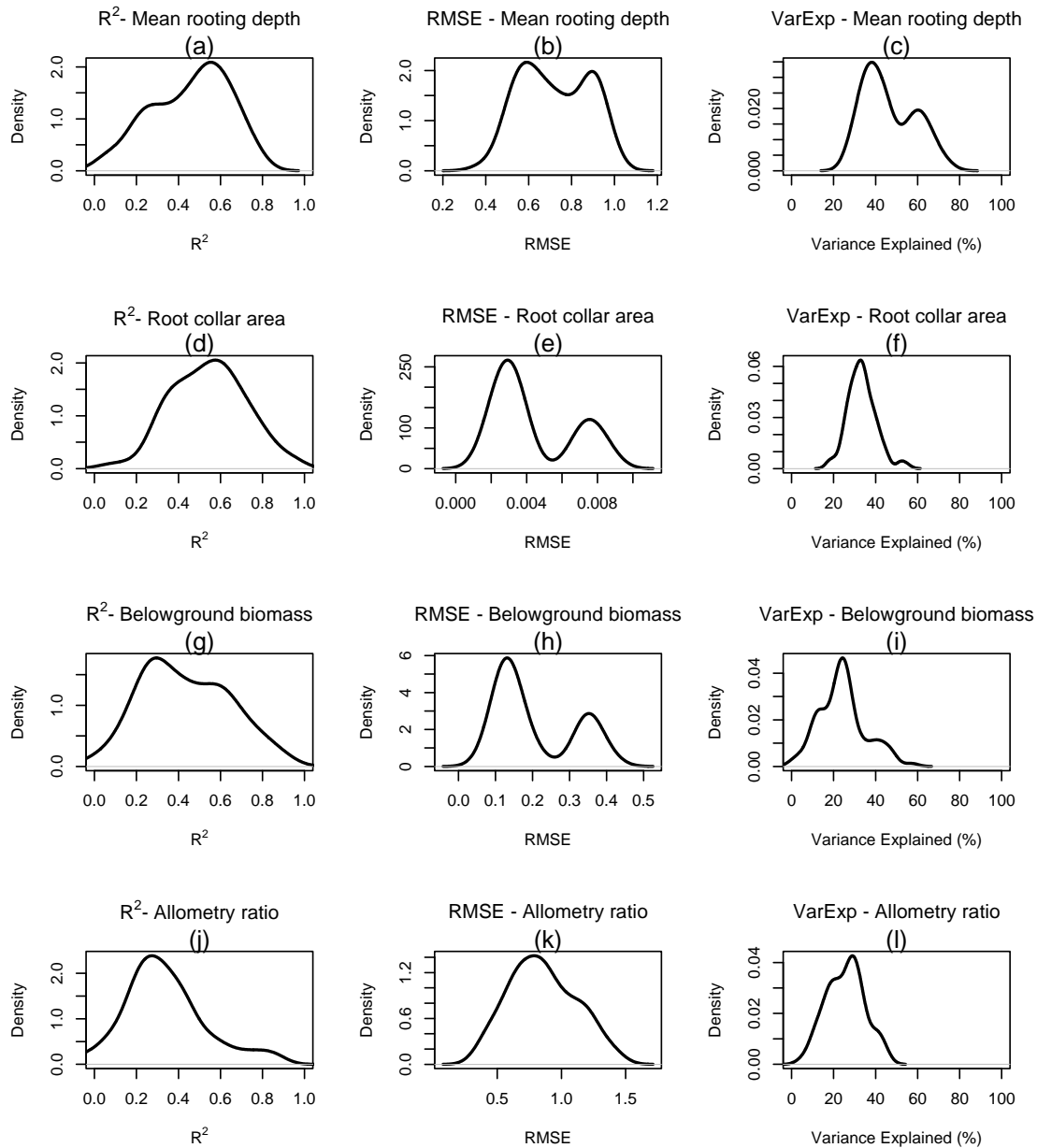
974 Zhang J, Wang J, Chen J, Song H, Li S, Zhao Y, Tao J and Liu J (2019) Soil Moisture
975 Determines Horizontal and Vertical Root Extension in the Perennial Grass *Lolium perenne* L.
976 Growing in Karst Soil. *Front. Plant Sci.* 10:629. doi: 10.3389/fpls.2019.00629

977 Zong, N, Song, M, Zhao, G, Shi, P., 2020. Nitrogen economy of alpine plants on the north
978 Tibetan Plateau: Nitrogen conservation by resorption rather than open sources through
979 biological symbiotic fixation. *Ecol Evol.* 2020; 10: 2051– 2061.
980 <https://doi.org/10.1002/ece3.6038>

981 Zuo, C., and R. Zhang (2002), Estimating root-water-uptake using an inverse method, *Soil*
982 *Sci.*, 167(9), 561– 571.

983

984 **Appendix A: Goodness of fit of the Random Forest models fitted to key vertical root**
 985 **distribution parameters**



986

987 *Figure A1. Probability density functions illustrating the coefficients of determination (R^2), root mean square error (RMSE) and*
 988 *variance explained (VarExp) retrieved from the cross-validation process implemented on random forest (RF) models, fitted*
 989 *between the studied soil and plant attributes to predict key vertical root distribution parameters.*

990

991

992

993

994 *Table A1. Coefficient of determination (R^2) and root mean square error (RMSE) for the best performing random forest*
995 *models fitted between the key vertical root distribution (VRD) parameters mean rooting depth (b), cross-sectional area at*
996 *the root collar (Aro) and root biomass (Mr) and the studied plant and soil attributes.*

	R^2	RMSE	Model No.
b	0.78	0.67	28
Aro	0.92	0.003	78
Mr	0.90	0.11	68

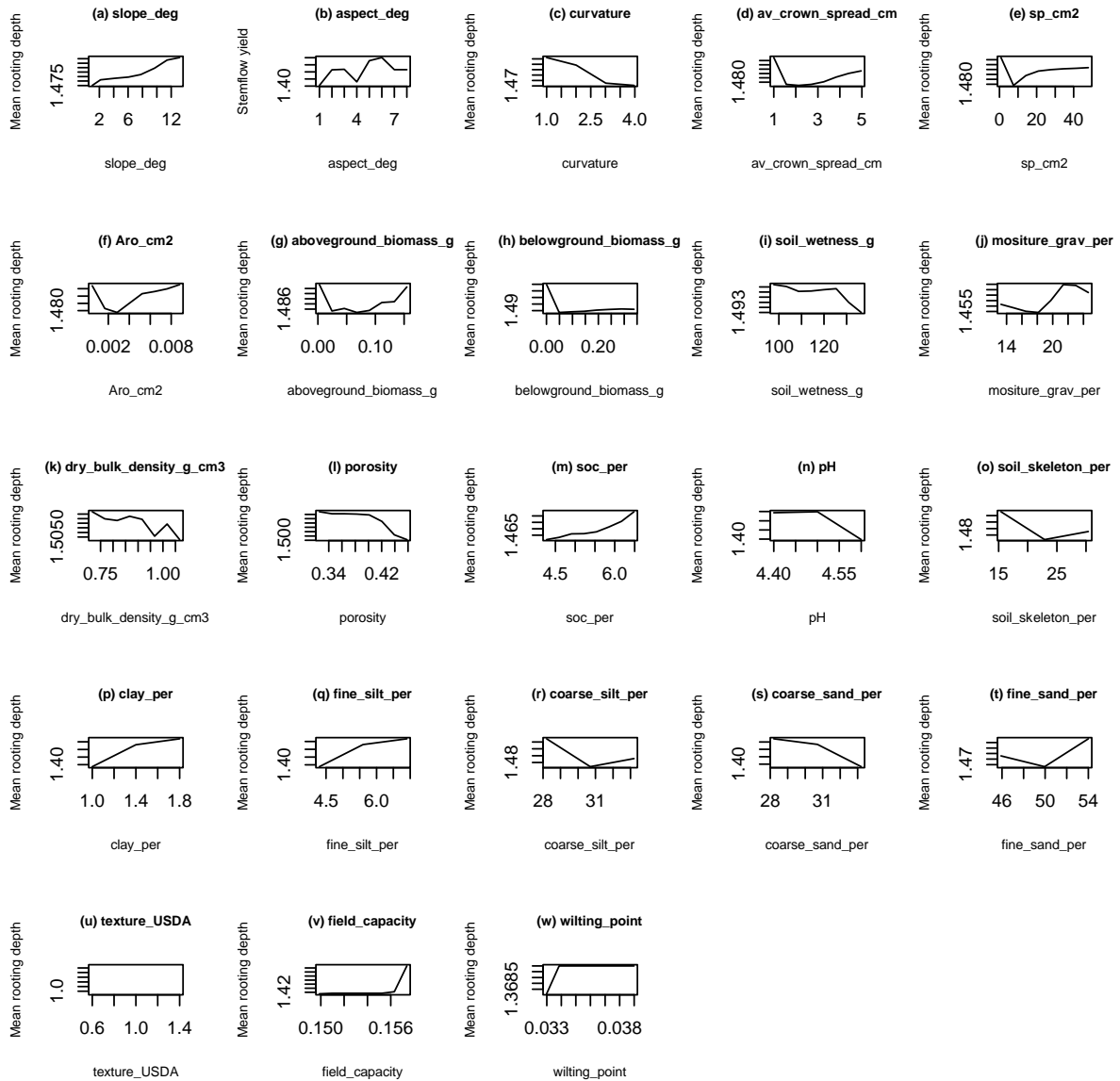
997

998

999 **Appendix B: Partial dependence plots (PDPs) for the key vertical root distribution**

1000 **parameters**

1001



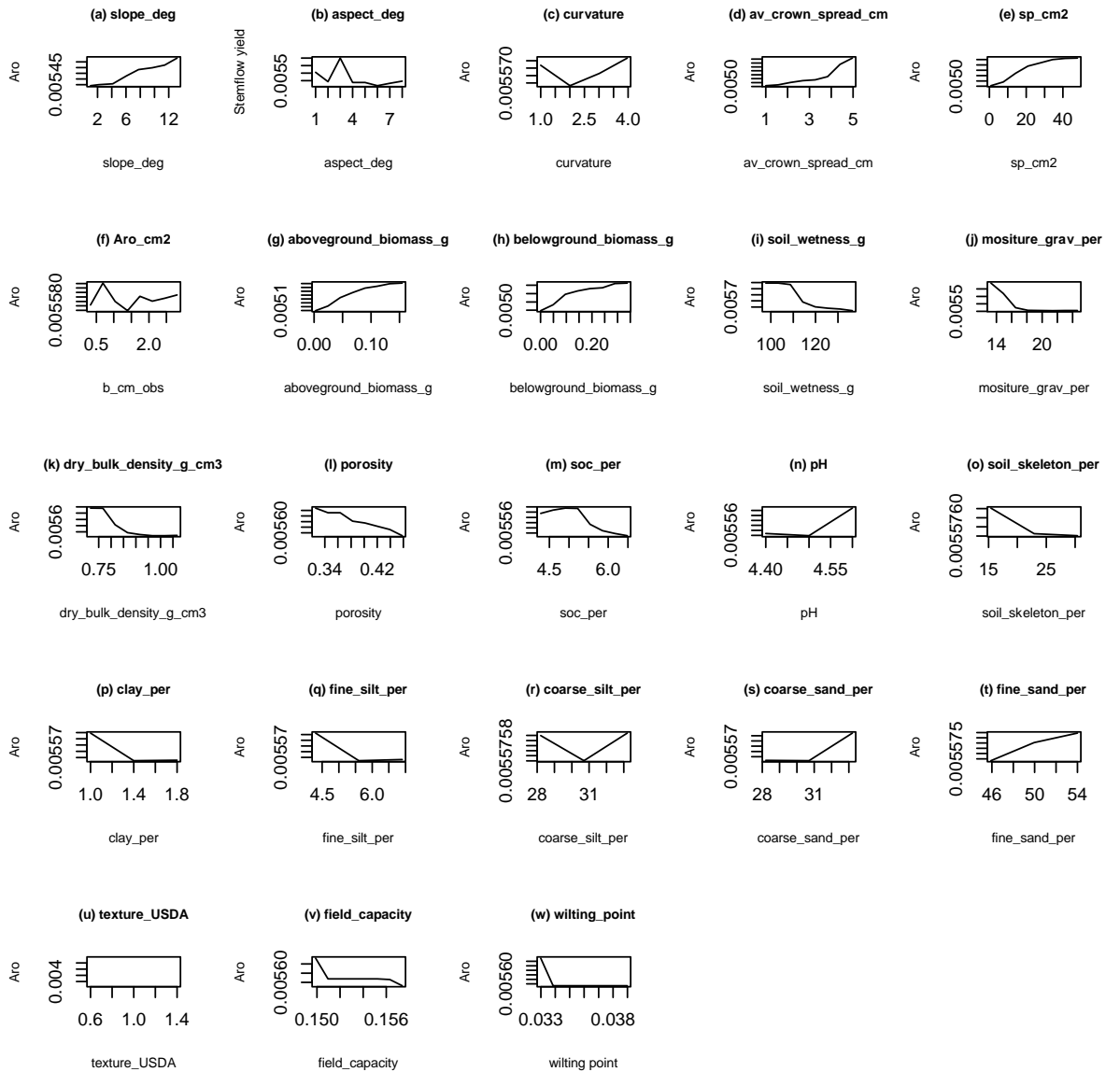
1002

1003 *Figure B1. Partial dependence plots (PDPs) showing the relationship between the mean rooting depth (b) and the investigated*
 1004 *plant and soil attributes in this study retrieved from fitting random forest models as indicated in the analytical framework*
 1005 *shown in Figure 4.*

1006

1007

1008



1009

1010 *Figure B2. Partial dependence plots (PDPs) showing the relationship between the cross-sectional area at the root collar (Aro)*
 1011 *and the investigated plant and soil attributes in this study retrieved from fitting random forest models as indicated in the*
 1012 *analytical framework shown in Figure 4.*

1013

1014

1015

1016

1017

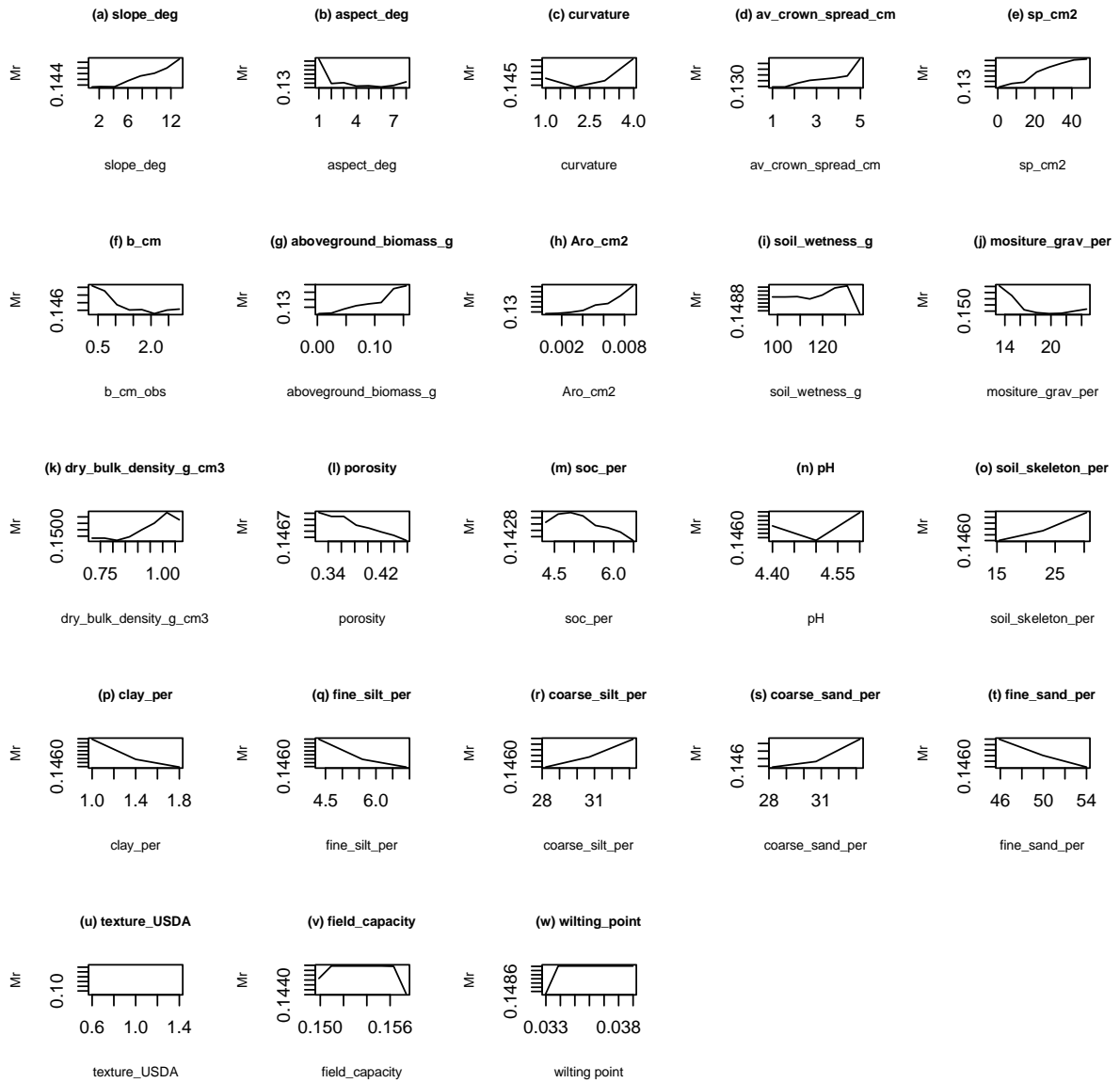


Figure B3. Partial dependence plots (PDPs) showing the relationship between the root biomass (Mr) and the investigated plant and soil attributes in this study retrieved from fitting random forest models as indicated in the analytical framework shown Figure 4.

1023

1024 Appendix C. R script – VRD data mining

```
1025 #Description:
1026 #this script provides a series of functions to evaluate the relationship between the 'rooting
1027 depth' variable and selected soil and plant attributes. Please, note that this is just a
1028 sample script for the 'rooting depth' only.
1029 #Instructions:
1030 #copy-paste the following script in your R console https://cran.r-project.org/ and change the
1031 working directory as appropriate
1032 #####
1033 #Outline
1034 #####
1035 #i-RANDOM FOREST IMPLEMENTATION: it fits random forest models (RF) between the target
1036 variable and selected plant and soil attributes and generates data frames storing relevant
1037 outputs related to goodness of fit and relative importance of covariates
1038 #ii-OUTPUTS COLLECTION AND RELATIVE IMPORTANCE EVALUATION: outputs collection, generation of
1039 output datasets and creation of relevant plots evaluating model quality
1040 #iii-PARTIAL DEPENDENCE PLOTS: creates practical dependence plots for the target variable
1041 #####
1042 #Abbreviations:
1043
1044 #b_cm_obs: measured mean rooting depth in cm
1045 #####
1046
1047
1048 #load data set and required R packages
1049
1050 setwd("/Users/ollauri/Desktop/work/catena_roots/in") #write the path to your folder here
1051 dts<-read.csv("DATASET.csv")
1052 library(caret)
1053 library(rattle)
1054 library(pdp)
1055 library(randomForest)
1056
1057 #~~~~~
1058 #i: RANDOM FOREST IMPLEMENTATION
1059 #~~~~~
1060
1061 n<-100 #number of models to fit
1062 RFs.b<-vector("list",n) #empty list object to store RF models
1063 predictions.b<-vector("list",n) #empty list object to store predictions from RF models
1064 train.A<-vector("list",n) #empty list object to store train data sets to fit RFs
1065 LMs.b<-vector("list",n) #empty list object to store objective function -i.e. linear
1066 regression models between observed and predicted
1067 RMSEs.b<-vector("list",n) #empty list to store RMSE (root mean square error)
1068 Rsq.b<-vector("list",n) #empty list to store coefficient of determination (r-sq)
1069 out.b<-list() #empty list to store outputs
1070 ct<-seq(1,100) #vector to assign numbers to outputs
1071 output.b<-matrix(,nrow=n,ncol=3) #empty matrix to store outputs
1072 varImp.b<-vector("list",n) #empty list to store variables importance
1073 varImp.vals.b<-list() #empty list to store values of relative importance
1074 varImp.names.b<-list() #empty list to store variables names related to relative importance
1075 for(i in 1:n){
1076   set.seed(i) #random number changes in each model run
1077   train.A[[i]]<-sample(nrow(dts),0.7*nrow(dts)) #sets training data set - i.e. bootstrapping
1078   RFs.b[[i]]<-randomForest(b_cm_obs~species+site+slope_deg+aspect_deg+curvature+
1079     av_crown_spread_cm+ sp_cm2+ Aro_cm2+aboveground_biomass_g+belowground_biomass_g+
1080     soil_wetness_g+ moisture_grav_per+ dry_bulk_density_g_cm3+ porosity+ soc_per+ pH+
1081     soil_skeleton_per+ clay_per+ fine_silt_per+ coarse_silt_per+ coarse_sand_per+ fine_sand_per+
1082     texture_USDA+ field_capacity+
1083     wilting_point,data=dts[train.A[[i]],,mtry=5,importance=TRUE,ntree=1000) #fits random forest
1084     models between target variable and soil & plant attributes
1085     predictions.b[[i]]<-predict(RFs.b[[i]],dts[-train.A[[i]],]) #predictions using the RF models
1086     and remaining data set
1087     LMs.b[[i]]<-lm(predictions.b[[i]]~dts$b_cm_obs[-train.A[[i]]) #fits regression models
1088     RMSEs.b[[i]]<-sqrt(mean((dts$b_cm_obs[-train.A[[i]]]-predictions.b[[i]])^2)) #calculates RMSE
1089     Rsq.b[[i]]<-as.matrix(summary(LMs.b[[i]])$adj.r.squared) #calculates r-sq
1090     out.b[[i]]<-list(ct[i],Rsq.b[[i]],RMSEs.b[[i]]) #stores outputs
1091     output.b[i,]<-c(out.b[[i]][[1]],as.numeric(out.b[[i]][[2]]),out.b[[i]][[3]]) #arranges
1092     outputs
1093     varImp.b[[i]]<-varImp(RFs.b[[i]]) #calculates RELATIVE IMPORTANCE
```

```

1095     varImp.vals.b[[i]]<-varImp.b[[i]] #stores relative importance values
1096     varImp.names.b[[i]]<-rownames(varImp.b[[i]])#stores variables names
1097 }
1098
1099
1100 #~~~~~
1101 #ii: OUTPUTS COLLECTION
1102 #~~~~~
1103 setwd("/Users/ollauri/Desktop/work/catena_roots/out")
1104 pdf("RFs_hist_rooting_depth_global.pdf")
1105 hist(output.b[,2],col="gray",main="b vs plant &
1106     soil",xlab=expression(paste("R"^2)),ylim=c(0,40)) #histogram showing density distribution
1107     function for goodness of fit of RF models
1108 dev.off()
1109 out.df.b<-data.frame(model=output.b[,1],Rsq=output.b[,2],RMSE=output.b[,3])
1110 write.csv(out.df.b,"b_global_RF.csv") #data frame storing summary for RF models' goodness of
1111     fit
1112 save(RFs.b,file="RFs_b_global.RData") #data base storing RF models
1113 varImp.df.b<-data.frame(var=unlist(varImp.names.b),imp=unlist(varImp.vals.b))
1114 write.csv(varImp.df.b,"varImp_b.csv") #data frame storing relative influence
1115 pdf("RFs_b_varImp.pdf")
1116 boxplot(imp~reorder(var,imp,FUN=mean),data=varImp.df.b,horizontal=TRUE,las=2,cex.axis=0.7,mai
1117     n="varImp rooting depth") #boxplot for relative influence
1118 dev.off()
1119
1120
1121
1122
1123
1124
1125 #~~~~~
1126 #iii: PARTIAL DEPENDENCE PLOTS
1127 #~~~~~
1128
1129 #Note: numerical variables, only - factor/character must be coded into numeric variables
1130     first
1131
1132
1133 #p1.x<-vector("list",n) #empty vectors to store partial dependence
1134 p2.x<-vector("list",n)
1135 p3.x<-vector("list",n)
1136 #p4.x<-vector("list",n)
1137 #p5.x<-vector("list",n)
1138 p6.x<-vector("list",n)
1139 p7.x<-vector("list",n)
1140 p8.x<-vector("list",n)
1141 p9.x<-vector("list",n)
1142 p10.x<-vector("list",n)
1143 p11.x<-vector("list",n)
1144 p12.x<-vector("list",n)
1145 p13.x<-vector("list",n)
1146 p14.x<-vector("list",n)
1147 p15.x<-vector("list",n)
1148 p16.x<-vector("list",n)
1149 p17.x<-vector("list",n)
1150 p18.x<-vector("list",n)
1151 p19.x<-vector("list",n)
1152 p20.x<-vector("list",n)
1153 p21.x<-vector("list",n)
1154 p22.x<-vector("list",n)
1155 #p23.x<-vector("list",n)
1156 p24.x<-vector("list",n)
1157 p25.x<-vector("list",n)
1158
1159 #store partial dependence for each covariate with the target variable
1160 for(i in 1:n){
1161 #p1.x[[i]]<-partial(RFs.b[[i]],pred.var="species",plot=FALSE,from=0,to=10)
1162 p2.x[[i]]<-partial(RFs.b[[i]],pred.var="site",plot=FALSE)
1163 p3.x[[i]]<-partial(RFs.b[[i]],pred.var="slope_deg",plot=FALSE)
1164 #p4.x[[i]]<-partial(RFs.b[[i]],pred.var="aspect_deg",plot=FALSE)
1165 #p5.x[[i]]<-partial(RFs.b[[i]],pred.var="curvature",plot=FALSE)
1166 p6.x[[i]]<-partial(RFs.b[[i]],pred.var="av_crown_spread_cm",plot=FALSE)
1167 p7.x[[i]]<-partial(RFs.b[[i]],pred.var="sp_cm2",plot=FALSE)
1168 p8.x[[i]]<-partial(RFs.b[[i]],pred.var="Aro_cm2",plot=FALSE)
1169 p9.x[[i]]<-partial(RFs.b[[i]],pred.var="aboveground_biomass_g",plot=FALSE)
1170 p10.x[[i]]<-partial(RFs.b[[i]],pred.var="belowground_biomass_g",plot=FALSE)
1171 p11.x[[i]]<-partial(RFs.b[[i]],pred.var="soil_wetness_g",plot=FALSE)

```

```

1172 p12.x[[i]]<-partial(RFs.b[[i]],pred.var="mositure_grav_per",plot=FALSE)
1173 p13.x[[i]]<-partial(RFs.b[[i]],pred.var="dry_bulk_density_g_cm3",plot=FALSE)
1174 p14.x[[i]]<-partial(RFs.b[[i]],pred.var="porosity",plot=FALSE)
1175 p15.x[[i]]<-partial(RFs.b[[i]],pred.var="soc_per",plot=FALSE)
1176 p16.x[[i]]<-partial(RFs.b[[i]],pred.var="pH",plot=FALSE)
1177 p17.x[[i]]<-partial(RFs.b[[i]],pred.var="soil_skeleton_per",plot=FALSE)
1178 p18.x[[i]]<-partial(RFs.b[[i]],pred.var="clay_per",plot=FALSE)
1179 p19.x[[i]]<-partial(RFs.b[[i]],pred.var="fine_silt_per",plot=FALSE)
1180 p20.x[[i]]<-partial(RFs.b[[i]],pred.var="coarse_silt_per",plot=FALSE)
1181 p21.x[[i]]<-partial(RFs.b[[i]],pred.var="coarse_sand_per",plot=FALSE)
1182 p22.x[[i]]<-partial(RFs.b[[i]],pred.var="fine_sand_per",plot=FALSE)
1183 #p23.x[[i]]<-partial(RFs.b[[i]],pred.var="texture_USDA",plot=FALSE)
1184 p24.x[[i]]<-partial(RFs.b[[i]],pred.var="field_capacity",plot=FALSE)
1185 p25.x[[i]]<-partial(RFs.b[[i]],pred.var="wilting_point",plot=FALSE)
1186 }
1187
1188 #retrieve outputs and arrange them for graphic display
1189
1190 #p1.a<-list()
1191 #for(i in 1:n){
1192 #   p1.a[[i]]<-p1.x[[i]][[1]]
1193 #}
1194 #p1.mtx.a<-do.call(rbind,p1.a)
1195 #p1.mtx.a.t<-t(p1.mtx.a)
1196 #p1.xs<-rowMeans(p1.mtx.a.t)
1197 #p1.b<-list()
1198 #for(i in 1:n){
1199 #   p1.b[[i]]<-p1.x[[i]][[2]]
1200 #}
1201
1202 #p1.mtx<-do.call(rbind,p1.b) #i kind of have now the list elements in a matrix
1203 #p1.mtx.t<-t(p1.mtx)
1204 #p1.yhat<-rowMeans(p1.mtx.t)
1205
1206 p2.a<-list()
1207 for(i in 1:n){
1208   p2.a[[i]]<-p2.x[[i]][[1]]
1209 }
1210 p2.mtx.a<-do.call(rbind,p2.a)
1211 p2.mtx.a.t<-t(p2.mtx.a)
1212 p2.xs<-rowMeans(p2.mtx.a.t)
1213 p2.b<-list()
1214 for(i in 1:n){
1215   p2.b[[i]]<-p2.x[[i]][[2]]
1216 }
1217 p2.mtx<-do.call(rbind,p2.b)
1218 p2.mtx.t<-t(p2.mtx)
1219 p2.yhat<-rowMeans(p2.mtx.t)
1220
1221 p3.a<-list()
1222 for(i in 1:n){
1223   p3.a[[i]]<-p3.x[[i]][[1]]
1224 }
1225 p3.mtx.a<-do.call(rbind,p3.a)
1226 p3.mtx.a.t<-t(p3.mtx.a)
1227 p3.xs<-rowMeans(p3.mtx.a.t)
1228 p3.b<-list()
1229 for(i in 1:n){
1230   p3.b[[i]]<-p3.x[[i]][[2]]
1231 }
1232 p3.mtx<-do.call(rbind,p3.b)
1233 p3.mtx.t<-t(p3.mtx)
1234 p3.yhat<-rowMeans(p3.mtx.t)
1235
1236 #p4.a<-list()
1237 #for(i in 1:n){
1238 #   p4.a[[i]]<-p4.x[[i]][[1]]
1239 #}
1240 #p4.mtx.a<-do.call(rbind,p4.a)
1241 #p4.mtx.a.t<-t(p4.mtx.a)
1242 #p4.xs<-rowMeans(p4.mtx.a.t)
1243 #p4.b<-list()
1244 #for(i in 1:n){
1245 #   p4.b[[i]]<-p4.x[[i]][[2]]
1246 #}
1247 #p4.mtx<-do.call(rbind,p4.b)
1248 #p4.mtx.t<-t(p4.mtx)

```

```

1249 #p4.yhat<-rowMeans(p4.mtx.t)
1250
1251 #p5.a<-list()
1252 #for(i in 1:n){
1253 #   p5.a[[i]]<-p5.x[[i]][[1]]
1254 #}
1255 #p5.mtx.a<-do.call(rbind,p5.a)
1256 #p5.mtx.a.t<-t(p5.mtx.a)
1257 #p5.xs<-rowMeans(p5.mtx.a.t)
1258 #p5.b<-list()
1259 #for(i in 1:n){
1260 #   p5.b[[i]]<-p5.x[[i]][[2]]
1261 #}
1262 #p5.mtx<-do.call(rbind,p5.b)
1263 #p5.mtx.t<-t(p5.mtx)
1264 #p5.yhat<-rowMeans(p5.mtx.t)
1265
1266 p6.a<-list()
1267 for(i in 1:n){
1268   p6.a[[i]]<-p6.x[[i]][[1]]
1269 }
1270 p6.mtx.a<-do.call(rbind,p6.a)
1271 p6.mtx.a.t<-t(p6.mtx.a)
1272 p6.xs<-rowMeans(p6.mtx.a.t)
1273 p6.b<-list()
1274 for(i in 1:n){
1275   p6.b[[i]]<-p6.x[[i]][[2]]
1276 }
1277 p6.mtx<-do.call(rbind,p6.b)
1278 p6.mtx.t<-t(p6.mtx)
1279 p6.yhat<-rowMeans(p6.mtx.t)
1280
1281 p7.a<-list()
1282 for(i in 1:n){
1283   p7.a[[i]]<-p7.x[[i]][[1]]
1284 }
1285 p7.mtx.a<-do.call(rbind,p7.a)
1286 p7.mtx.a.t<-t(p7.mtx.a)
1287 p7.xs<-rowMeans(p7.mtx.a.t)
1288 p7.b<-list()
1289 for(i in 1:n){
1290   p7.b[[i]]<-p7.x[[i]][[2]]
1291 }
1292 p7.mtx<-do.call(rbind,p7.b)
1293 p7.mtx.t<-t(p7.mtx)
1294 p7.yhat<-rowMeans(p7.mtx.t)
1295
1296 p8.a<-list()
1297 for(i in 1:n){
1298   p8.a[[i]]<-p8.x[[i]][[1]]
1299 }
1300 p8.mtx.a<-do.call(rbind,p8.a)
1301 p8.mtx.a.t<-t(p8.mtx.a)
1302 p8.xs<-rowMeans(p8.mtx.a.t)
1303 p8.b<-list()
1304 for(i in 1:n){
1305   p8.b[[i]]<-p8.x[[i]][[2]]
1306 }
1307 p8.mtx<-do.call(rbind,p8.b)
1308 p8.mtx.t<-t(p8.mtx)
1309 p8.yhat<-rowMeans(p8.mtx.t)
1310
1311 p9.a<-list()
1312 for(i in 1:n){
1313   p9.a[[i]]<-p9.x[[i]][[1]]
1314 }
1315 p9.mtx.a<-do.call(rbind,p9.a)
1316 p9.mtx.a.t<-t(p9.mtx.a)
1317 p9.xs<-rowMeans(p9.mtx.a.t)
1318 p9.b<-list()
1319 for(i in 1:n){
1320   p9.b[[i]]<-p9.x[[i]][[2]]
1321 }
1322 p9.mtx<-do.call(rbind,p9.b)
1323 p9.mtx.t<-t(p9.mtx)
1324 p9.yhat<-rowMeans(p9.mtx.t)
1325

```

```

1326 p10.a<-list()
1327 for(i in 1:n){
1328   p10.a[[i]]<-p10.x[[i]][[1]]
1329 }
1330 p10.mtx.a<-do.call(rbind,p10.a)
1331 p10.mtx.a.t<-t(p10.mtx.a)
1332 p10.xs<-rowMeans(p10.mtx.a.t)
1333 p10.b<-list()
1334 for(i in 1:n){
1335   p10.b[[i]]<-p10.x[[i]][[2]]
1336 }
1337 p10.mtx<-do.call(rbind,p10.b)
1338 p10.mtx.t<-t(p10.mtx)
1339 p10.yhat<-rowMeans(p10.mtx.t)
1340
1341 p11.a<-list()
1342 for(i in 1:n){
1343   p11.a[[i]]<-p11.x[[i]][[1]]
1344 }
1345 p11.mtx.a<-do.call(rbind,p11.a)
1346 p11.mtx.a.t<-t(p11.mtx.a)
1347 p11.xs<-rowMeans(p11.mtx.a.t)
1348 p11.b<-list()
1349 for(i in 1:n){
1350   p11.b[[i]]<-p11.x[[i]][[2]]
1351 }
1352 p11.mtx<-do.call(rbind,p11.b)
1353 p11.mtx.t<-t(p11.mtx)
1354 p11.yhat<-rowMeans(p11.mtx.t)
1355
1356 p12.a<-list()
1357 for(i in 1:n){
1358   p12.a[[i]]<-p12.x[[i]][[1]]
1359 }
1360 p12.mtx.a<-do.call(rbind,p12.a)
1361 p12.mtx.a.t<-t(p12.mtx.a)
1362 p12.xs<-rowMeans(p12.mtx.a.t)
1363 p12.b<-list()
1364 for(i in 1:n){
1365   p12.b[[i]]<-p12.x[[i]][[2]]
1366 }
1367 p12.mtx<-do.call(rbind,p12.b)
1368 p12.mtx.t<-t(p12.mtx)
1369 p12.yhat<-rowMeans(p12.mtx.t)
1370
1371 p13.a<-list()
1372 for(i in 1:n){
1373   p13.a[[i]]<-p13.x[[i]][[1]]
1374 }
1375 p13.mtx.a<-do.call(rbind,p13.a)
1376 p13.mtx.a.t<-t(p13.mtx.a)
1377 p13.xs<-rowMeans(p13.mtx.a.t)
1378 p13.b<-list()
1379 for(i in 1:n){
1380   p13.b[[i]]<-p13.x[[i]][[2]]
1381 }
1382 p13.mtx<-do.call(rbind,p13.b)
1383 p13.mtx.t<-t(p13.mtx)
1384 p13.yhat<-rowMeans(p13.mtx.t)
1385
1386 p14.a<-list()
1387 for(i in 1:n){
1388   p14.a[[i]]<-p14.x[[i]][[1]]
1389 }
1390 p14.mtx.a<-do.call(rbind,p14.a)
1391 p14.mtx.a.t<-t(p14.mtx.a)
1392 p14.xs<-rowMeans(p14.mtx.a.t)
1393 p14.b<-list()
1394 for(i in 1:n){
1395   p14.b[[i]]<-p14.x[[i]][[2]]
1396 }
1397 p14.mtx<-do.call(rbind,p14.b)
1398 p14.mtx.t<-t(p14.mtx)
1399 p14.yhat<-rowMeans(p14.mtx.t)
1400
1401 p15.a<-list()
1402 for(i in 1:n){

```

```

1403   p15.a[[i]]<-p15.x[[i]][[1]]
1404   }
1405   p15.mtx.a<-do.call(rbind,p15.a)
1406   p15.mtx.a.t<-t(p15.mtx.a)
1407   p15.xs<-rowMeans(p15.mtx.a.t)
1408   p15.b<-list()
1409   for(i in 1:n){
1410     p15.b[[i]]<-p15.x[[i]][[2]]
1411   }
1412   p15.mtx<-do.call(rbind,p15.b)
1413   p15.mtx.t<-t(p15.mtx)
1414   p15.yhat<-rowMeans(p15.mtx.t)
1415
1416
1417   p16.a<-list()
1418   for(i in 1:n){
1419     p16.a[[i]]<-p16.x[[i]][[1]]
1420   }
1421   p16.mtx.a<-do.call(rbind,p16.a)
1422   p16.mtx.a.t<-t(p16.mtx.a)
1423   p16.xs<-rowMeans(p16.mtx.a.t)
1424   p16.b<-list()
1425   for(i in 1:n){
1426     p16.b[[i]]<-p16.x[[i]][[2]]
1427   }
1428   p16.mtx<-do.call(rbind,p16.b)
1429   p16.mtx.t<-t(p16.mtx)
1430   p16.yhat<-rowMeans(p16.mtx.t)
1431
1432
1433   p17.a<-list()
1434   for(i in 1:n){
1435     p17.a[[i]]<-p17.x[[i]][[1]]
1436   }
1437   p17.mtx.a<-do.call(rbind,p17.a)
1438   p17.mtx.a.t<-t(p17.mtx.a)
1439   p17.xs<-rowMeans(p17.mtx.a.t)
1440   p17.b<-list()
1441   for(i in 1:n){
1442     p17.b[[i]]<-p17.x[[i]][[2]]
1443   }
1444   p17.mtx<-do.call(rbind,p17.b)
1445   p17.mtx.t<-t(p17.mtx)
1446   p17.yhat<-rowMeans(p17.mtx.t)
1447
1448
1449   p18.a<-list()
1450   for(i in 1:n){
1451     p18.a[[i]]<-p18.x[[i]][[1]]
1452   }
1453   p18.mtx.a<-do.call(rbind,p18.a)
1454   p18.mtx.a.t<-t(p18.mtx.a)
1455   p18.xs<-rowMeans(p18.mtx.a.t)
1456   p18.b<-list()
1457   for(i in 1:n){
1458     p18.b[[i]]<-p18.x[[i]][[2]]
1459   }
1460   p18.mtx<-do.call(rbind,p18.b)
1461   p18.mtx.t<-t(p18.mtx)
1462   p18.yhat<-rowMeans(p18.mtx.t)
1463
1464
1465   p19.a<-list()
1466   for(i in 1:n){
1467     p19.a[[i]]<-p19.x[[i]][[1]]
1468   }
1469   p19.mtx.a<-do.call(rbind,p19.a)
1470   p19.mtx.a.t<-t(p19.mtx.a)
1471   p19.xs<-rowMeans(p19.mtx.a.t)
1472   p19.b<-list()
1473   for(i in 1:n){
1474     p19.b[[i]]<-p19.x[[i]][[2]]
1475   }
1476   p19.mtx<-do.call(rbind,p19.b)
1477   p19.mtx.t<-t(p19.mtx)
1478   p19.yhat<-rowMeans(p19.mtx.t)
1479
1480
1481   p20.a<-list()
1482   for(i in 1:n){
1483     p20.a[[i]]<-p20.x[[i]][[1]]

```



```

1480 }
1481 p20.mtx.a<-do.call(rbind,p20.a)
1482 p20.mtx.a.t<-t(p20.mtx.a)
1483 p20.xs<-rowMeans(p20.mtx.a.t)
1484 p20.b<-list()
1485 for(i in 1:n){
1486   p20.b[[i]]<-p20.x[[i]][[2]]
1487 }
1488 p20.mtx<-do.call(rbind,p20.b)
1489 p20.mtx.t<-t(p20.mtx)
1490 p20.yhat<-rowMeans(p20.mtx.t)
1491
1492 p21.a<-list()
1493 for(i in 1:n){
1494   p21.a[[i]]<-p21.x[[i]][[1]]
1495 }
1496 p21.mtx.a<-do.call(rbind,p21.a)
1497 p21.mtx.a.t<-t(p21.mtx.a)
1498 p21.xs<-rowMeans(p21.mtx.a.t)
1499 p21.b<-list()
1500 for(i in 1:n){
1501   p21.b[[i]]<-p21.x[[i]][[2]]
1502 }
1503 p21.mtx<-do.call(rbind,p21.b)
1504 p21.mtx.t<-t(p21.mtx)
1505 p21.yhat<-rowMeans(p21.mtx.t)
1506
1507 p22.a<-list()
1508 for(i in 1:n){
1509   p22.a[[i]]<-p22.x[[i]][[1]]
1510 }
1511 p22.mtx.a<-do.call(rbind,p22.a)
1512 p22.mtx.a.t<-t(p22.mtx.a)
1513 p22.xs<-rowMeans(p22.mtx.a.t)
1514 p22.b<-list()
1515 for(i in 1:n){
1516   p22.b[[i]]<-p22.x[[i]][[2]]
1517 }
1518 p22.mtx<-do.call(rbind,p22.b)
1519 p22.mtx.t<-t(p22.mtx)
1520 p22.yhat<-rowMeans(p22.mtx.t)
1521
1522 #p23.a<-list()
1523 #for(i in 1:n){
1524 #   p23.a[[i]]<-p23.x[[i]][[1]]
1525 #}
1526 #p23.mtx.a<-do.call(rbind,p23.a)
1527 #p23.mtx.a.t<-t(p23.mtx.a)
1528 #p23.xs<-rowMeans(p23.mtx.a.t)
1529 #p23.b<-list()
1530 #for(i in 1:n){
1531 #   p23.b[[i]]<-p23.x[[i]][[2]]
1532 #}
1533 #p23.mtx<-do.call(rbind,p23.b)
1534 #p23.mtx.t<-t(p23.mtx)
1535 #p23.yhat<-rowMeans(p23.mtx.t)
1536
1537 p24.a<-list()
1538 for(i in 1:n){
1539   p24.a[[i]]<-p24.x[[i]][[1]]
1540 }
1541 p24.mtx.a<-do.call(rbind,p24.a)
1542 p24.mtx.a.t<-t(p24.mtx.a)
1543 p24.xs<-rowMeans(p24.mtx.a.t)
1544 p24.b<-list()
1545 for(i in 1:n){
1546   p24.b[[i]]<-p24.x[[i]][[2]]
1547 }
1548 p24.mtx<-do.call(rbind,p24.b)
1549 p24.mtx.t<-t(p24.mtx)
1550 p24.yhat<-rowMeans(p24.mtx.t)
1551
1552 p25.a<-list()
1553 for(i in 1:n){
1554   p25.a[[i]]<-p25.x[[i]][[1]]
1555 }
1556 p25.mtx.a<-do.call(rbind,p25.a)

```

```

1557 p25.mtx.a.t<-t(p25.mtx.a)
1558 p25.xs<-rowMeans(p25.mtx.a.t)
1559 p25.b<-list()
1560 for(i in 1:n){
1561   p25.b[[i]]<-p25.x[[i]][[2]]
1562 }
1563 p25.mtx<-do.call(rbind,p25.b)
1564 p25.mtx.t<-t(p25.mtx)
1565 p25.yhat<-rowMeans(p25.mtx.t)
1566
1567 #plot PDPs
1568
1569
1570 pdf("RFs_rooting_depth_PDPs.pdf")
1571 par(mfrow=c(5,5))
1572 #plot(p1.yhat[1:8]~p1.xs[1:8],type="l",xlab="species",ylab="Mean rooting depth",main="(a)
1573   species",cex.main=0.8,cex.lab=0.8)
1574 plot(p2.yhat[1:8]~p2.xs[1:8],type="l",xlab="site",ylab="Mean rooting depth",main="(b)
1575   site",cex.main=0.8,cex.lab=0.8)
1576 plot(p3.yhat[1:8]~p3.xs[1:8],type="l",xlab="slope_deg",ylab="Mean rooting depth",main="(c)
1577   slope_deg",cex.main=0.8,cex.lab=0.8)
1578 #plot(p4.yhat[1:8]~p4.xs[1:8],type="l",xlab="aspect_deg",ylab="Mean rooting depth",main="(d)
1579   aspect_deg",cex.main=0.8,cex.lab=0.8)
1580 #plot(p5.yhat[1:8]~p5.xs[1:8],type="l",xlab="curvature",ylab="Mean rooting depth",main="(e)
1581   curvature",cex.main=0.8,cex.lab=0.8)
1582 plot(p6.yhat[1:8]~p6.xs[1:8],type="l",xlab="av_crown_spread_cm",ylab="Mean rooting
1583   depth",main="(f) av_crown_spread_cm",cex.main=0.8,cex.lab=0.8)
1584 plot(p7.yhat[1:8]~p7.xs[1:8],type="l",xlab="sp_cm2",ylab="Mean rooting depth",main="(g)
1585   sp_cm2",cex.main=0.8,cex.lab=0.8)
1586 plot(p8.yhat[1:8]~p8.xs[1:8],type="l",xlab="Aro_cm2",ylab="Mean rooting depth",main="(h)
1587   Aro_cm2",cex.main=0.8,cex.lab=0.8)
1588 plot(p9.yhat[1:8]~p9.xs[1:8],type="l",xlab="aboveground_biomass_g",ylab="Mean rooting
1589   depth",main="(i) aboveground_biomass_g",cex.main=0.8,cex.lab=0.8)
1590 plot(p10.yhat[1:8]~p10.xs[1:8],type="l",xlab="belowground_biomass_g",ylab="Mean rooting
1591   depth",main="(j) belowground_biomass_g",cex.main=0.8,cex.lab=0.8)
1592 plot(p11.yhat[1:8]~p11.xs[1:8],type="l",xlab="soil_wetness_g",ylab="Mean rooting
1593   depth",main="(k) soil_wetness_g",cex.main=0.8,cex.lab=0.8)
1594 plot(p12.yhat[1:8]~p12.xs[1:8],type="l",xlab="mositure_grav_per",ylab="Mean rooting
1595   depth",main="(l) mositure_grav_per",cex.main=0.8,cex.lab=0.8)
1596 plot(p13.yhat[1:8]~p13.xs[1:8],type="l",xlab="dry_bulk_density_g_cm3",ylab="Mean rooting
1597   depth",main="(m) dry_bulk_density_g_cm3",cex.main=0.8,cex.lab=0.8)
1598 plot(p14.yhat[1:8]~p14.xs[1:8],type="l",xlab="porosity",ylab="Mean rooting depth",main="(n)
1599   porosity",cex.main=0.8,cex.lab=0.8)
1600 plot(p15.yhat[1:8]~p15.xs[1:8],type="l",xlab="soc_per",ylab="Mean rooting depth",main="(o)
1601   soc_per",cex.main=0.8,cex.lab=0.8)
1602 plot(p16.yhat[1:8]~p16.xs[1:8],type="l",xlab="pH",ylab="Mean rooting depth",main="(p)
1603   pH",cex.main=0.8,cex.lab=0.8)
1604 plot(p17.yhat[1:8]~p17.xs[1:8],type="l",xlab="soil_skeleton_per",ylab="Mean rooting
1605   depth",main="(p) soil_skeleton_per",cex.main=0.8,cex.lab=0.8)
1606 plot(p18.yhat[1:8]~p18.xs[1:8],type="l",xlab="clay_per",ylab="Mean rooting depth",main="(p)
1607   clay_per",cex.main=0.8,cex.lab=0.8)
1608 plot(p19.yhat[1:8]~p19.xs[1:8],type="l",xlab="fine_silt_per",ylab="Mean rooting
1609   depth",main="(p) fine_silt_per",cex.main=0.8,cex.lab=0.8)
1610 plot(p20.yhat[1:8]~p21.xs[1:8],type="l",xlab="coarse_silt_per",ylab="Mean rooting
1611   depth",main="(p) coarse_silt_per",cex.main=0.8,cex.lab=0.8)
1612 plot(p21.yhat[1:8]~p21.xs[1:8],type="l",xlab="coarse_sand_per",ylab="Mean rooting
1613   depth",main="(p) coarse_sand_per",cex.main=0.8,cex.lab=0.8)
1614 plot(p22.yhat[1:8]~p22.xs[1:8],type="l",xlab="fine_sand_per",ylab="Mean rooting
1615   depth",main="(p) fine_sand_per",cex.main=0.8,cex.lab=0.8)
1616 #plot(p23.yhat[1:8]~p23.xs[1:8],type="l",xlab="texture_USDA",ylab="Mean rooting
1617   depth",main="(p) texture_USDA",cex.main=0.8,cex.lab=0.8)
1618 plot(p24.yhat[1:8]~p24.xs[1:8],type="l",xlab="field_capacity",ylab="Mean rooting
1619   depth",main="(p) field_capacity",cex.main=0.8,cex.lab=0.8)
1620 plot(p25.yhat[1:8]~p25.xs[1:8],type="l",xlab="wilting_point",ylab="Mean rooting
1621   depth",main="(p) wilting_point",cex.main=0.8,cex.lab=0.8)
1622 dev.off()
1623
1624

```

1625